scientific reports

Check for updates

OPEN

# Preparation and evaluation of temozolomide loaded PLGA nanoparticles for the treatment of glioblastoma multiforme

Şule Şahin[1], Elif Kaya-Tilki[2], Merve Baysal[3] & A. Alper Öztürk[1]✉

**Glioblastoma multiforme (GBM) remains one of the most lethal primary brain tumors, with limited treatment options and poor patient prognosis. Although temozolomide (TMZ) is the standard chemotherapeutic agent for GBM, its clinical efficacy is severely hindered by rapid systemic clearance, low brain penetration, and non-selective cytotoxicity. In this study, we developed and comparatively evaluated two innovative PLGA-based nanoparticle (NP) systems for oral TMZ delivery, prepared via nanoprecipitation and double emulsion solvent evaporation techniques. Comprehensive physicochemical characterization, including particle size, polydispersity index (PDI), zeta potential (ZP), encapsulation efficiency (EE%), in vitro release kinetics, and solid-state analysis (DSC and FTIR), demonstrated the successful formation of nanosystems with favorable properties. NP1-TMZ (nanoprecipitation) showed superior characteristics, including smaller particle size, narrower size distribution, higher encapsulation efficiency, and more efficient cellular uptake compared to NP2-TMZ (double emulsion). Moreover, cytotoxicity studies in U-87 MG glioblastoma and NIH/3T3 fibroblast cell lines revealed enhanced tumor selectivity and reactive oxygen species (ROS) generation for NP1-TMZ, highlighting its potential for selective tumor targeting. Our results demonstrate that optimized nanoencapsulation significantly improves TMZ delivery, stability, and therapeutic performance, offering a promising strategy for next-generation GBM treatments.**

**Keywords** Glioblastoma, Temozolomide, Nanoprecipitation, Double emulsion solvent evaporation, PLGA nanoparticles, Oral chemotherapy, Drug release, Reactive oxygen species

Glioblastoma (GBM) represents the most prevalent and malignant form of primary brain tumors, characterized by its rapid progression and poor prognosis. According to epidemiological data, the median overall survival for patients diagnosed with GBM typically ranges between 12 and 15 months, despite current therapeutic approaches. The World Health Organization (WHO) has classified GBM as a grade IV tumor, indicating its highly aggressive and infiltrative nature. The standard first-line treatment regimen involves maximal safe surgical resection to reduce tumor burden, followed by a combination of radiotherapy and concurrent chemotherapy, most commonly with temozolomide (TMZ). Nevertheless, treatment remains largely palliative, and recurrence is almost inevitable, underscoring the urgent need for more effective therapeutic strategies[1,2].

TMZ is an oral alkylating chemotherapeutic agent that is structurally derived from dacarbazine. Its mechanism of action is primarily based on its ability to methylate DNA at the O6 position of guanine, thereby inducing apoptosis in rapidly dividing cancer cells. TMZ exhibits excellent oral bioavailability and is rapidly absorbed into the systemic circulation following administration. One of the pharmacological advantages of TMZ is its ability to cross the blood-brain barrier (BBB) due to its small molecular weight and lipophilic nature, making it a more favorable chemotherapeutic option for central nervous system malignancies compared to other alkylating agents. The U.S. Food and Drug Administration (FDA) approved TMZ in 2005 as part of the standard treatment protocol for GBM. In addition to GBM, TMZ has shown therapeutic benefit in the management of other aggressive and treatment-resistant solid tumors, such as advanced neuroendocrine tumors, due to its broad-spectrum antitumor activity and favorable pharmacokinetic profile[3–5]. Despite its promising anticancer activity, TMZ suffers from several pharmacokinetic and physicochemical limitations that

[1]Department of Pharmaceutical Technology, Faculty of Pharmacy, Anadolu University, Eskişehir, Türkiye. [2]Department of Pharmacology, Faculty of Pharmacy, Anadolu University, Eskişehir, Türkiye. [3]Department of Pharmaceutical Toxicology, Faculty of Pharmacy, Anadolu University, Eskişehir, Türkiye. ✉email: aaozturk@anadolu.edu.tr

significantly hinder its clinical efficacy. One of the major drawbacks is its short biological half-life, typically ranging between 1.8 and 2 h, which leads to rapid elimination from the body. Additionally, TMZ is highly susceptible to pH-dependent hydrolysis, a process that occurs swiftly under physiological conditions, resulting in the transformation of TMZ into inactive metabolites such as MTIC (3-methyl-(triazen-1-yl)imidazole-4-carboxamide) and AIC (5-aminoimidazole-4-carboxamide). These degradation products possess limited cell permeability and reduced cytotoxic potential, thereby compromising the drug's overall therapeutic efficacy. However, despite its BBB permeability, pharmacokinetic studies have shown that only a small fraction—less than 1%—of the orally administered dose reaches the brain parenchyma in its active form, which limits its therapeutic efficacy. To compensate for this poor brain bioavailability, clinicians often resort to administering high systemic doses, which in turn results in dose-dependent adverse effects, most notably hematological toxicities such as myelosuppression and thrombocytopenia[6,7]. Additionally, when the studies are examined, one of the biggest difficulties is the lack of selectivity towards cancer cells in chemotherapy[8].

To address these challenges, various advanced drug delivery strategies have been investigated. Among them, the encapsulation of TMZ in nanoscale carriers—including organic systems like liposomes, polymeric nanoparticles (NPs), dendrimers, and micelles, as well as inorganic nanomaterials such as mesoporous silica, gold, silver, and quantum dots—has demonstrated improved drug stability, prolonged circulation time, and enhanced brain accumulation. In parallel, the conjugation of TMZ with small molecules or polymers has been explored to enhance its physicochemical properties, cellular uptake, and targeted delivery, representing a promising avenue for overcoming the current limitations associated with conventional TMZ therapy[9–13].

The development of new therapeutic compounds is not only expensive and time-consuming, but also involves multiple complex stages that are often prone to failure. As an alternative to this challenging process, enhancing the pharmacological properties—such as bioavailability, selectivity, efficacy, and safety—of drugs that are already in clinical use may offer a more efficient and practical solution. In recent years, researchers have extensively investigated a range of innovative strategies to optimize existing therapies. These include stimulus-responsive targeted delivery systems, drug–polymer conjugates, NP-mediated drug carriers, personalized treatment regimens, and therapeutic drug monitoring approaches[14,15].

In recent years, NP-based carrier systems have garnered significant interest as a means to address various therapeutic challenges. These systems are solid colloidal carriers ranging from 10 to 1000 nanometers in size, and can be fabricated using natural or synthetic polymers, as well as inorganic or ceramic materials. The active pharmaceutical ingredient can be incorporated into NPs in several ways: it may be dissolved or dispersed within the particle matrix, adsorbed onto the surface, or chemically linked via covalent bonding. NPs are generally classified into two main types: nanospheres, in which the active compound is uniformly distributed throughout the polymer matrix, and nanocapsules, where the active substance is confined within a core surrounded by a polymeric shell[16].

Poly(lactic-co-glycolic acid) (PLGA), a widely utilized polymer in nanomedicine, has been approved by both FDA and the European Medicines Agency (EMA) for use in targeted chemotherapy applications. As a commonly employed structural and core component in NP formulations, PLGA offers several notable advantages, including excellent biodegradability, biocompatibility, and the capacity for extensive surface modification. These tunable properties make it highly suitable for the development of NP-based drug delivery systems aimed at improving therapeutic efficacy and specificity[17–20]. In this study, both double emulsion solvent evaporation and nanoprecipitation methods were utilized for the preparation of PLGA-based NPs intended for oral administration. Double emulsion solvent evaporation is a widely applied technique that enables effective encapsulation of hydrophilic drugs, offering high encapsulation efficiency and controllable particle size, which are essential for achieving reproducible release profiles in oral formulations. Conversely, nanoprecipitation is a simpler and more rapid technique that facilitates the production of uniformly distributed, small-sized NPs with excellent stability. This method is particularly advantageous when a narrow particle size distribution and high drug loading are required. By applying both approaches in parallel, we were able to directly compare their influence on critical formulation parameters such as particle size, polydispersity, and encapsulation efficiency, thereby identifying their respective strengths for enhancing the oral bioavailability of TMZ.

In the present study, a dual formulation strategy was employed by preparing TMZ-loaded PLGA NPs using both double emulsion solvent evaporation and nanoprecipitation techniques—allowing for a direct comparison of their impact on critical physicochemical parameters such as particle size, polydispersity index (PDI), zeta potential, encapsulation efficiency, and release profile. The resulting NPs were comprehensively characterized using FTIR and DSC analyses to confirm drug incorporation, polymer–drug compatibility, and physical state transitions. To confirm the successful formation and molecular dispersion of TMZ within the PLGA NPs, complementary characterization techniques such as DLS, DSC, and FT-IR were employed. Beyond formulation development, the study advances existing approaches by integrating in vitro selectivity assessments using both cancerous (U-87 MG) and non-cancerous (NIH3T3) cell lines. By evaluating intracellular ROS (reactive oxygen species) generation, a key indicator of oxidative stress-mediated cytotoxicity, the selective toxicity potential of the formulations toward glioblastoma cells was elucidated. This combined strategy highlights the potential of nanoencapsulation not only to improve the oral bioavailability of TMZ, but also to enhance tumor-specific activity, offering a promising and translationally relevant alternative to conventional chemotherapy.

## Materials and methods

### Materials

TMZ used in this study was kindly gifted by Deva Holding (Istanbul, Türkiye). Resomer RG 502 H (PLGA) and sodium hydroxide, were obtained from Sigma-Aldrich (USA). PVA (polyvinyl alcohol) and potassium phosphate monobasic were also obtained from Sigma-Aldrich (Germany). Acetone AND Dimethylformamide were sourced from Merck (Germany). Deionized water was used in all experiments (Milli-Q Academic,

| Code | Organic phase | | | | Water phase PVA solution 10 mL | Preparation/Device Condition |
|---|---|---|---|---|---|---|
| | PLGA | TMZ | DMF | Span 60 | | Dropping speed |
| NP1-Blank | 60 mg | – | 3 mL | 20 mg | %1.5 (w/v) | 5 mL.h$^{-1}$ |
| NP1-TMZ | 60 mg | 6 mg | 3 mL | 20 mg | %1.5 (w/v) | 5 mL.h$^{-1}$ |

**Table 1**. Composition of PLGA-Based NP formulations prepared by nanoprecipitation technique.

| Code | Water phase ($W_1$) | | Oil phase ($O_1$) | | Water phase ($W_2$) | Preparation/Device Condition | |
|---|---|---|---|---|---|---|---|
| | PBS pH 7.4 containing 1.5% (w/v) PVA | TMZ | PLGA | Acetone | PBS pH 7.4 containing 1.5% (w/v) PVA | Probe sonication power (Amplitude) | Probe sonication time (Seconds) |
| NP2-Blank | 400 µL | – | 60 mg | 3 mL | 10 mL | %60 | 90 |
| NP2-TMZ | 400 µL | 6 mg | 60 mg | 3 mL | 10 mL | %60 | 90 |

**Table 2**. Composition of PLGA-Based NP formulations prepared by double emulsion solvent evaporation technique.

Millipore, Molsheim, France). U-87 MG (HTB-14) and NIH/3T3 (CRL-1658) cell lines were purchased from the American Type Culture Collection (ATCC, Manassas, VA, USA). All other chemicals were of analytical grade.

## Preparation of NP formulations

NPs were formulated using modified versions of the nanoprecipitation (solvent displacement) and double emulsion solvent evaporation techniques[18,19,21–23].

*Preparation of PLGA-based nanoparticles via nanoprecipitation technique*

PLGA-based NPs were prepared using a modified nanoprecipitation (solvent displacement) technique. Briefly, an accurately weighed amount of PLGA was dissolved in 3 mL of dimethylformamide (DMF) containing Span 60 as a stabilizer. This organic phase was then added dropwise at a rate of 5 mL·h$^{-1}$ into 10 mL of an aqueous polyvinyl alcohol (PVA) solution (1.5% w/v) under continuous magnetic stirring. Following complete addition, the organic solvent was removed using a rotary evaporator. The resulting NP suspension was centrifuged at 11.000 rpm for 45 min at 4 °C to collect the NPs. The NPs were redispersed in 5 mL of distilled water and washed by repeating the centrifugation step two additional times to ensure the removal of unentrapped materials and residual solvents. For the preparation of TMZ-loaded NPs, 6 mg of TMZ was dissolved into the organic phase prior to the nanoprecipitation step. Following the washing steps, the NPs were resuspended in distilled water, frozen, and subsequently lyophilized for further use. Detailed compositions of the PLGA-based formulations developed via the nanoprecipitation technique are summarized in Table 1.

*Preparation of PLGA-based nanoparticles via double emulsion solvent evaporation technique*

PLGA-based NPs were also prepared using a modified double emulsion solvent evaporation ($W_1/O/W_2$) technique. Briefly, 60 mg of PLGA was accurately weighed and dissolved in 3 mL of acetone to form the organic phase. Subsequently, 400 µL of an aqueous PBS solution (pH 7.4) containing 1.5% (w/v) PVA was added dropwise into the organic phase under ultrasonication (1 min, ultrasonic bath) to obtain a primary water-in-oil ($W_1/O$) emulsion. This primary emulsion was then slowly added to 10 mL of an external aqueous phase containing 1.5% (w/v) PVA in PBS (pH 7.4) and emulsified using a probe sonicator (Sonics, USA) operating at 60% amplitude for 90 s to form the double emulsion ($W_1/O/W_2$). The organic solvent was evaporated at room temperature under continuous stirring for 4 h. The resulting NP dispersion was centrifuged at 11.000 rpm for 45 min at 4 °C. The obtained NPs were washed twice with distilled water, redispersed, frozen, and lyophilized using a freeze-dryer to obtain a dry powder. For the preparation of TMZ-loaded NPs, TMZ was dissolved in the inner aqueous phase (400 µL PBS, pH 7.4, containing 1% PVA) prior to emulsification. Detailed compositions of the PLGA-based formulations developed via the double emulsion solvent evaporation technique are summarized in Table 2.

## Particle size, polydispersity index (PDI), and zeta potential

The particle size (PS) and polydispersity index (PDI) of the NP formulations were determined by dynamic light scattering (DLS) using a Zetasizer Nano-ZS (Malvern Panalytical, Malvern, UK). Zeta potential (ZP) measurements were also conducted using the same instrument. For PS and PDI analysis, the NPs were appropriately diluted with distilled water and measured at 25 °C. ZP values were determined using a disposable folded capillary zeta cell under identical temperature conditions, following dilution with distilled water to ensure proper conductivity. Each sample was analyzed in triplicate, and the results were reported as mean ± standard deviation (Mean ± SD).

## UV-visible spectrophotometric method

For in vitro studies, the quantification of TMZ was conducted using a UV-visible spectrophotometer. Two separate validation studies were performed for encapsulation efficiency (EE%) and in vitro release assessments[24–26]. The UV-visible spectrophotometric analysis was performed at 327 nm using a quartz cuvette and a UV-160 A UV/Vis

recording spectrophotometer (Shimadzu). Analytical validation studies were conducted for TMZ quantification in both encapsulation efficiency (EE%) and in vitro dissolution tests. For this purpose, two different solvent systems were employed: a DMF: water mixture (1:1, v/v) for EE%, and phosphate-buffered saline (PBS, pH 7.4) for dissolution studies. Initially, a standard TMZ stock solution with a final concentration of 1000 μg.mL$^{-1}$ was prepared in each medium. Calibration curves were constructed using six concentrations (2.5, 5.0, 7.5, 10.0, 15.0, and 20.0 μg.mL$^{-1}$) and evaluated using linear regression (least squares method). Precision was assessed through intra-day and inter-day replicates at three concentrations (5.0, 10.0, and 15.0 μg.mL$^{-1}$), and accuracy was evaluated by spiking known amounts of standard TMZ into the samples. For selectivity and specificity, spectral comparisons were made between TMZ, the solvent system (DMF: water or PBS), and blank formulations (NP1-Blank and NP2-Blank) over the 200–800 nm range.

## Encapsulation efficiency

The encapsulation efficiency (EE%) of TMZ in NP1-TMZ and NP2-TMZ formulations was determined by quantifying the amount of drug extracted from the NPs. For each measurement, 5 mg of lyophilized NP powder was accurately weighed and placed into a suitable container. Then, 1 mL of an DMF: water mixture (1:1, v/v) was added to dissolve the NPs, followed by vortexing for 5 min to ensure complete disruption of the polymer matrix and release of the encapsulated TMZ. The resulting solution was filtered through a 0.22 μm membrane filter to eliminate any residual polymer particles. After appropriate dilution, the concentration of TMZ in the filtrate was determined using a UV–visible spectrophotometer at 327 nm. All analyses were performed in triplicate, and the EE% was calculated as the percentage of the initial theoretical drug content successfully encapsulated within the NPs (Eq. 1).

$$EE\,\% = \left( \frac{Amount\ of\ TEM\ encapsulated}{Theoretical\ amount\ of\ TEM\ in\ the\ NP} \right) \times\ 100 \tag{1}$$

## In vitro release

The in vitro release profiles of pure TMZ, NP1-TMZ, and NP2-TMZ formulations were evaluated using the dialysis bag diffusion technique. Briefly, lyophilized NP formulations—containing an amount equivalent to 5 mg of TMZ—as well as 5 mg of pure TMZ were separately transferred into dialysis membrane bags (cellulose tubing, MWCO: 14,000 Da; flat width: 33 mm; D9652, Sigma-Aldrich) pre-filled with 3 mL of phosphate-buffered saline (PBS, pH 7.4). Each dialysis bag was then immersed into 100 mL of release medium (PBS, pH 7.4) maintained at 37 ± 1 °C and stirred at 100 rpm in a thermostatically controlled shaker. To minimize medium evaporation, the receptor compartments were tightly sealed throughout the experiment. At predetermined time intervals (1, 2, 3, 4, 5, 6, 7, 9, 12, 24, 48, and 72 h), 3 mL of the release medium was withdrawn and immediately replaced with an equal volume of fresh, pre-warmed PBS. The amount of TMZ released at each time point was determined using a UV–visible spectrophotometer at 327 nm. All measurements were performed in triplicate for each group, and the results were expressed as mean ± standard deviation (SD). The cumulative percentage of drug release was plotted as a function of time to generate release profiles for comparative analysis.

## Release kinetics

After obtaining the release profiles, data were transferred to the DDSolver program to determine the most important and popular criteria: coefficient of determination ($R^2$), adjusted coefficient of determination ($R^2$adjusted), Akaike Information Criterion (AIC), Model Selection Criterion (MSC) etc. The highest $R^2$, $R^2$ adjusted and MSC values and the lowest AIC values were used for evaluating Higuchi, Korsmeyer-Peppas, and Weibull models. Finally, release differences of NP1-TMZ and prepared NP2-TMZ were evaluated by DDSolver according to 'Similarity Factor' (f2)[27–30].

## Solid-state characterization

*Thermal analysis*

The thermal behavior of the samples was evaluated using a differential scanning calorimeter (DSC-60; Shimadzu Scientific Instruments, Columbia, MI, USA). Approximately 5 mg of each sample was accurately weighed and sealed in an aluminum crucible. The analysis was performed over a temperature range of 30–300 °C with a heating rate of 10 °C/min, under a continuous air flow of 50 mL/min. In addition to the TMZ-loaded NP formulations (NP1-TMZ and NP2-TMZ), reference samples including pure TMZ, PLGA, and blank NPs (NP1-Blank and NP2-Blank) were analyzed for comparative purposes to assess potential interactions between the drug and polymer matrix as well as possible changes in the physical state of the drug[31,32].

*Fourier-transform infrared spectroscopy (FT-IR) analysis*

FTIR analyses were performed using a Shimadzu IR Prestige-21 spectrophotometer (Shimadzu Corporation, Kyoto, Japan) in the spectral range of 4000–500 cm$^{-1}$. In addition to the TMZ-loaded NP formulations (NP1-TMZ and NP2-TMZ), reference samples including pure TMZ, PLGA, and blank NPs (NP1-Blank and NP2-Blank) were also evaluated for comparative analysis. The spectra were assessed to identify potential shifts or disappearance of characteristic peaks, which may indicate physical interactions or chemical compatibility between the drug and polymer matrix[31–33].

## U-87 MG and NIH/3T3 cell culture

U-87 MG (HTB-14) and NIH/3T3 (CRL-1658) cell lines were purchased from the American Type Culture Collection (ATCC, Manassas, VA, USA). U-87 MG human glioblastoma and NIH3T3 mouse fibroblast cell lines

were cultured in Dulbecco's Modified Eagle's Medium (DMEM) at 37 °C within a humidified incubator containing 5% $CO_2$ and 10% fetal bovine serum (FBS), along with 1% penicillin/streptomycin. The cells underwent passages and were either transferred to new flasks or prepared as cell stocks for subsequent experiments once they reached a proliferation density of 70–80%. Prior to the experiments, cell counts were performed using the TC20 Automated Cell Counter (Bio-Rad, USA) after staining with trypan blue solution to confirm the appropriate cell numbers.

### MTT cell viability assay

The anti-cancer and cytotoxic properties of TMZ, NP1-TMZ, NP2-TMZ, NP1-Blank, and NP2-Blank were assessed through a colorimetric assay on 96-well plates using MTT (3-(4,5-Dimethylthiazol-2-yl)−2,5-Diphenyltetrazolium Bromide) reagent on U-87 MG and NIH/3T3 cells, respectively. The MTT assay measures cell viability by assessing the reduction of a yellow tetrazolium salt (MTT) to a purple formazan product within metabolically active cells. This colorimetric reaction provides a quantitative indication of cellular health and proliferation, with higher absorbance values correlating to increased cell viability[34]. To assess the effect of the samples, cells were initially plated at a density of $10 \times 10^{-3}$ cells per well in 96-well plates. After 24 h, the wells were treated with varying concentrations (1, 10, 100, and 400 $\mu g.mL^{-1}$) of the samples and incubated for an additional 24 h. Subsequently, 10 µL of MTT solution was added to each well, and after a 3-hour incubation period, absorbances were measured at 540 nm using a BioTek Synergy H1 Multimode Reader (BioTek, USA). The recorded absorbance directly correlates with the number of viable cells, and cell viability rates were expressed as a percentage of the control value[35–37].

The selectivity indexes were calculated by the ratio of the $IC_{50}$ values obtained for normal cells to the $IC_{50}$ values of cancer cells. The selectivity index values greater than 1 indicate preferred selectivity toward cancer cells[38].

### The determination of reactive oxygen species (ROS) generation

The DCFDA/H2DCFDA cellular reactive oxygen species (ROS) assay kit (Abcam PLC, Cambridge, MA) was used to measure hydroxyl, peroxyl and other intracellular ROS activity within the cell[39]. The kit was utilized following the instructions provided by the manufacturer. Briefly, the cells were planted in a 96-well plate at 2.5 × 104 cells/100 µL well and incubated for 24 h at 37 °C. Then the medium was removed and 100 µL DCFDA (20 µM) solution was added to each well and incubated for 45 min. After that, the DCFDA solution was removed, and wells were washed with 1X buffer. The different concentrations of the compounds (1, 10, 100, and 400 $\mu g.mL^{-1}$) were added. The intensity of the fluorescence was measured using a fluorescence plate reader (excitation: 485 nm/emission: 535 nm) for 4 h in the time intervals of 30 min.

## Results and discussion

### Particle size, polydispersity index (PDI), and zeta potential

As shown in Table 3; Fig. 1., the mean particle size (PS) of the NP1-Blank and NP1-TMZ formulations was found to be 142.100 ± 1.114 nm and 142.467 ± 1.132 nm, respectively, indicating no statistically significant difference between the blank and drug-loaded NPs within the NP1 group. However, a statistically significant increase in PS was observed between NP1 and NP2 formulations (NP1-TMZ vs. NP2-TMZ, $p < 0.001$), suggesting that the double emulsion solvent evaporation method used for NP2 may result in larger PSs compared to the nanoprecipitation method. Although there was no statistically significant difference between NP2-Blank (149.933 ± 1.976 nm) and NP2-TMZ (153.867 ± 3.365 nm), a numerical increase in PS was observed upon drug loading[14,18]. This trend has also been reported in previous studies and can be explained by several formulation-related factors[21–23,40]. First, the incorporation of the active compound into the NP structure may increase the core volume, leading to a moderate enlargement in size. The drug may occupy space within the polymer matrix, which contributes to the observed change. Second, changes in surface properties after drug loading may influence colloidal stability. These changes can affect the hydrodynamic diameter measured by DLS, even without visible aggregation. Finally, in techniques like double emulsion solvent evaporation, the presence of the drug can impact emulsification efficiency. Variations in internal phase composition, such as increased viscosity, may result in slightly larger particles. In summary, although the size increase was not statistically significant, it is consistent with literature findings and can be attributed to physical and structural changes associated with drug encapsulation[41–43]. Crossing the blood-brain barrier (BBB) is an important point in brain tumors and many other diseases related to the brain. There are data reported in the literature that effective GBM treatment can be achieved with NPs with particle sizes between 100 and 200 nm[44,45]. When the PS results obtained in this study are evaluated, they can be considered as formulations that are compatible with the literature and may be used in the treatment of GMB. Figure 2. also presents particle size distribution graphs from the Zetasizer.

| Code | PS, nm (mean ± SD) | PDI (mean ± SD) | ZP, mV (mean ± SD) | EE % (mean ± SD) |
|---|---|---|---|---|
| NP1-Blank | 142.100 ± 1.114 | 0.134 ± 0.022 | −9.787 ± 0.065 | – |
| NP1-TMZ | 142.467 ± 1.132 | 0.159 ± 0.009 | −9.140 ± 0.298 | 70.02 ± 2.6 |
| NP2-Blank | 149.933 ± 1.976 | 0.220 ± 0.008 | −7.967 ± 0.164 | – |
| NP2-TMZ | 153.867 ± 3.365 | 0.254 ± 0.006 | −7.913 ± 0.118 | 54.63 ± 3.1 |

**Table 3**. Particle Size, polydispersity index (PDI), zeta potential, and encapsulation efficiency (EE %) results.

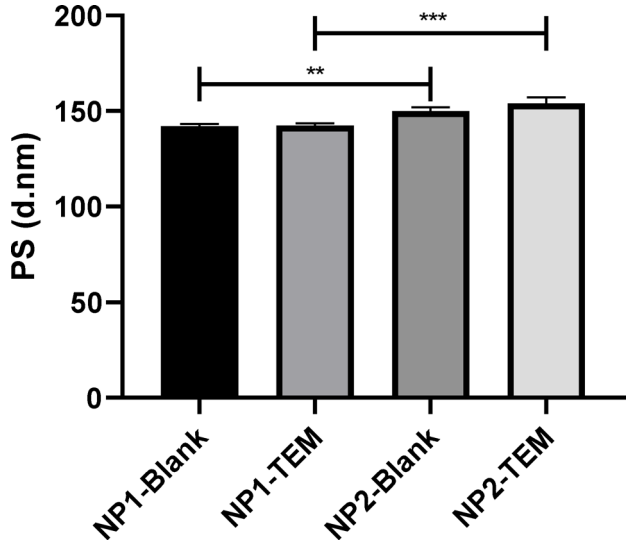



**Fig. 1**. Statistical evaluation of the particle size results. (Significant differences are indicated as *p < 0.05, **p < 0.01, ***p < 0.001, ****p < 0.0001, while no significant difference is represented as p > 0.05 or ns).

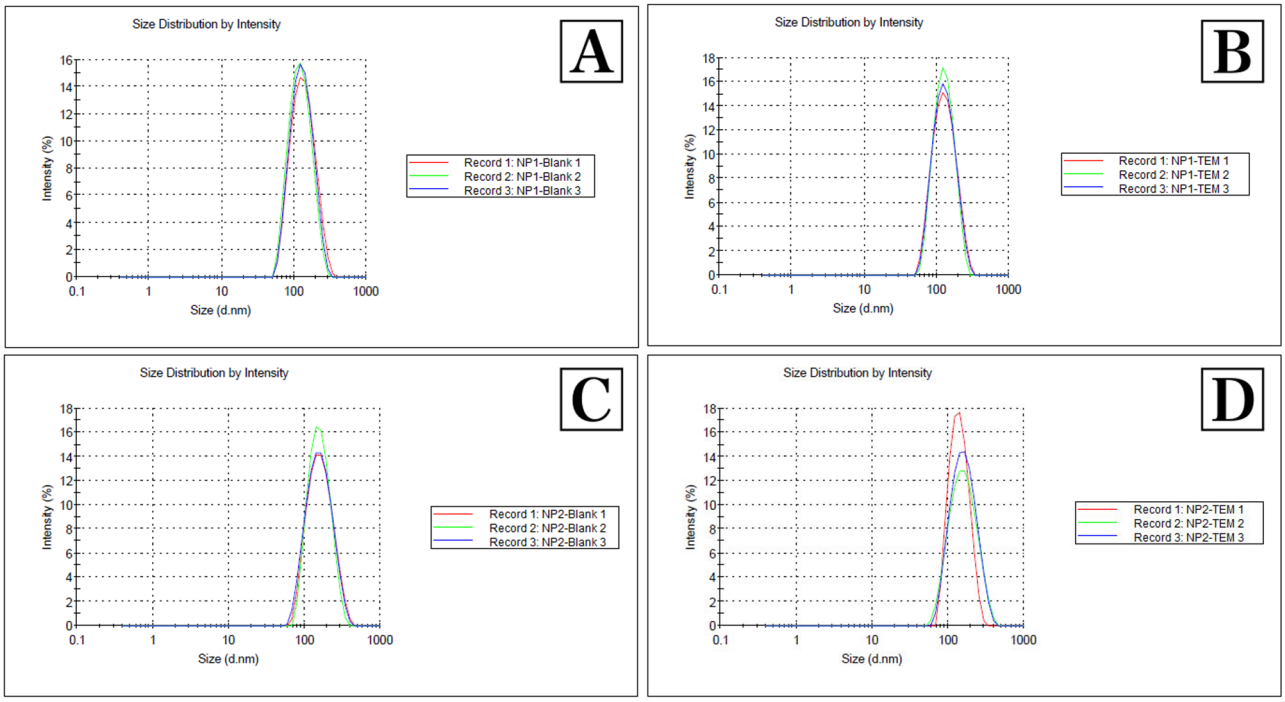



**Fig. 2**. Particle size distribution profiles of the nanoparticle formulations recorded by dynamic light scattering (DLS) using the Zetasizer Nano ZS. **A** Particle size distribution graph of NP1-Blank formulation; **B** Particle size distribution graph of NP1-TMZ formulation; **C** Particle size distribution graph of NP2-Blank formulation; **D** Particle size distribution graph of NP2-TMZ formulation.

Polydispersity index (PDI) results, presented in Table 3; Fig. 3., demonstrate a clear trend of increasing heterogeneity in PS distribution, particularly for the NP2 group. The PDI of NP1 formulations remained below 0.2 (NP1-Blank: 0.134 ± 0.022; NP1-TMZ: 0.159 ± 0.009), indicating a relatively narrow size distribution and homogenous particle population. In contrast, both NP2-Blank (0.220 ± 0.008) and NP2-TMZ (0.254 ± 0.006) showed significantly higher PDI values, suggesting that the double emulsion method may yield more polydisperse systems. The statistically significant increase between NP2-Blank and NP2-TMZ ($p < 0.05$) implies that drug loading further contributes to PS variability, possibly due to phase separation or instability during solvent removal. This is particularly important when considering formulation reproducibility and scalability.

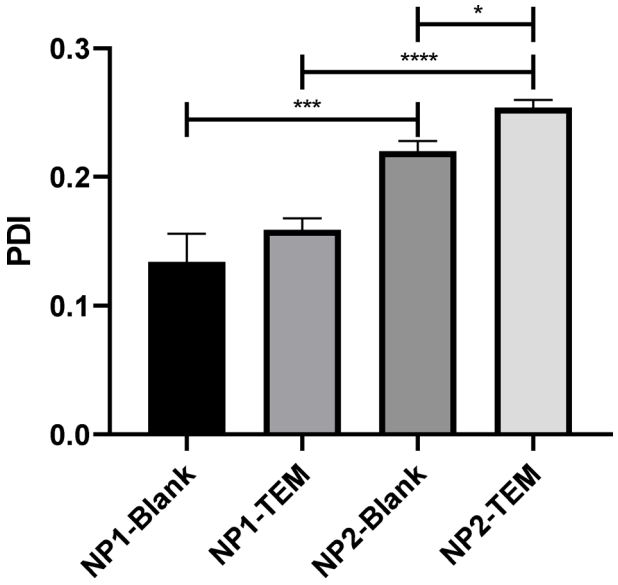



**Fig. 3**. Statistical evaluation of the PDI results. (Significant differences are indicated as *p < 0.05, **p < 0.01, ***p < 0.001, ****p < 0.0001, while no significant difference is represented as p > 0.05 or ns).

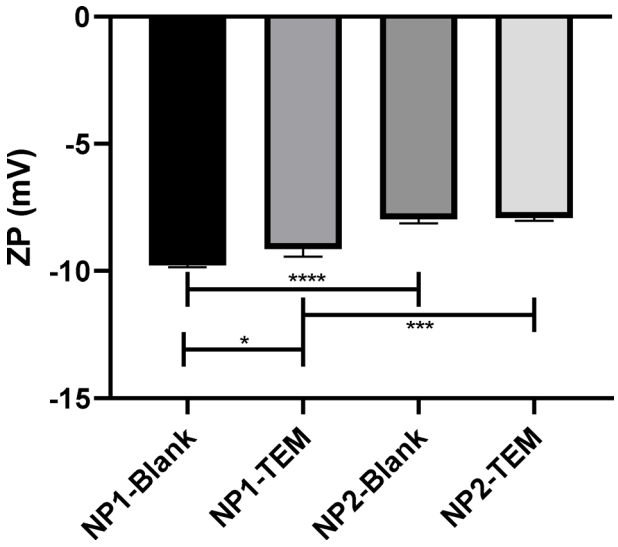



**Fig. 4**. Statistical evaluation of the zeta potential results. (Significant differences are indicated as *p < 0.05, **p < 0.01, ***p < 0.001, ****p < 0.0001, while no significant difference is represented as p > 0.05 or ns).

Although a PDI value below 0.5 is generally considered acceptable for NP formulations, values below 0.3 are regarded as optimal, indicating a more uniform PS distribution. In this study, all formulations exhibited PDI values within the acceptable range, confirming the successful preparation of monodisperse systems. Moreover, the nanoprecipitation method yielded NPs with lower PDI values compared to the double emulsion technique, suggesting its superiority in producing more homogeneous NP populations[46–48].

Zeta potential (ZP) values depicted in Table 3; Fig. 4. reveal that all formulations possessed negative surface charges, ranging between −7.913 and −9.787 mV. ZP values of NPs were found to be negative resulting from the total negative charges of chemical groups on PLGA polymer in water[49]. NP1-Blank had the highest negative charge (−9.787 ± 0.065 mV), while NP2-TMZ displayed the least negative value (−7.913 ± 0.118 mV). Statistically significant differences were observed between several groups: NP1-Blank vs. NP1-TMZ: $p < 0.05$, NP1-Blank vs. NP2-Blank: $p < 0.0001$, NP1-TMZ vs. NP2-TMZ: $p < 0.001$. These results suggest that both the preparation method and the presence of the active compound influence surface charge. The less negative ZP in NP2 groups may reflect surfactant adsorption differences or encapsulation-associated surface rearrangements. Although absolute ZP values are moderate, they remain within an acceptable range for colloidal stability in short-term studies; however, additional stabilization strategies might be required for long-term storage. Previous

studies have shown that zeta potential values between − 5.0 and − 15.0 mV are considered to be at the threshold of flocculation in nanosystems, with values in the range of − 5.0 to − 3.0 mV indicating a maximum tendency for flocculation[40,50]. Based on the measured ZP values and previously established thresholds for colloidal stability, it can be concluded that the NPs prepared in this study exhibit a relatively stable profile, with sufficient surface charge to prevent immediate flocculation under the tested conditions.

Although the ZP values of the formulations were relatively low, the very small PDI values indicate that monodisperse and stable nanosystems were successfully obtained. This suggests that, despite limited electrostatic repulsion, sufficient colloidal stability was achieved, potentially due to steric stabilization provided by the PLGA polymer matrix. Additionally, the presence of a polymeric layer may have shifted the shear plane, resulting in a lower measured zeta potential without compromising NP stability[51–53].

In general, nanosystems with smaller PSs are favored for effective penetration across the blood-brain barrier (BBB). In our study, the ability of the developed NP formulations to traverse the BBB can be attributed primarily to their nanoscale dimensions and surface charge characteristics, which support both passive diffusion and endocytosis-mediated transport mechanisms. It has been reported that NPs smaller than 200 nm can cross the BBB via transcytosis pathways, including adsorptive-mediated and receptor-mediated transport. The negative ZP observed in our formulations contributes to colloidal stability by reducing the risk of aggregation during systemic circulation, thus supporting efficient delivery to the brain. These physicochemical properties collectively suggest that the developed PLGA-based nanosystem may enhance the brain bioavailability of the encapsulated agent, ultimately improving its therapeutic potential in GBM treatment[54–57]. Taken together, the results indicate that the nanoprecipitation method (NP1) provides more uniform and smaller particles with better surface charge characteristics compared to the double emulsion solvent evaporation method (NP2). The increase in size and polydispersity upon drug loading in NP2 suggests a potential formulation challenge that may affect bioavailability and in vivo performance. For this reason, NP2-TMZ may be preferred as an optimum formulation with better properties.

## UV-visible spectrophotometric method

The UV-visible spectrophotometric method developed for the quantitative determination of EE% was validated in an DMF-water (1:1, v/v) medium. The linearity study yielded a regression equation of $y = 0.049x + 0.0019$ ($r^2 = 0.9999$) within the concentration range of 2.5–20.0 $\mu g.mL^{-1}$. The relative standard deviation (%RSD) for precision at three concentration levels (5.0, 10.0, and 15.0 $\mu g.mL^{-1}$) was found to be below 2%, demonstrating the method's precision. Accuracy assessment results for the UV-visible spectrophotometric method were 99.967 ± 0.624%, 99.943 ± 0.312%, and 99.935 ± 0.136% for 5.0, 10.0, and 15.0 $\mu g.mL^{-1}$, respectively. In the selectivity analysis, blank formulations (NP1-Blank and NP-Blank) and the DMF-water (1:1, v/v) mixture were scanned between 200 and 800 nm, showing no absorbance peaks at 327 nm, confirming the specificity of the method. The limit of detection (LOD) and limit of quantification (LOQ) were determined as 0.182 $\mu g.mL^{-1}$and 0.553 $\mu g.mL^{-1}$, respectively, which were lower than the minimum concentration evaluated in the linearity study, further supporting the method's suitability.

For in vitro release studies, the UV-visible spectrophotometric method was validated in PBS (pH 7.4) as the medium. The regression equation was established as $y = 0.0049x - 0.0031$ ($r^2 = 0.9999$) within the concentration range of 2.5–20.0 $\mu g.mL^{-1}$. The precision assessment indicated that %RSD values for the 5.0, 10.0, and 15.0 µg/mL samples were below 2%, confirming the method's reproducibility. Accuracy values for the spectrophotometric method were calculated as 100.187 ± 0.623%, 100.113 ± 0.408%, and 100.678 ± 0.208% for the respective concentrations. The selectivity study revealed that blank formulations (NP1-Blank and NP-Blank) and PBS (pH 7.4), when analyzed between 200 and 800 nm, did not exhibit any absorbance peaks at 327 nm, ensuring the specificity of the method. The LOD and LOQ values were determined to be 0.177 µg/mL and 0.537 $\mu g.mL^{-1}$, respectively, both of which were below the lowest concentration assessed in the linearity study, further validating the method's reliability.

In conclusion, the two spectrophotometric methods developed in this study offer simple, cost-effective, and reliable approaches for the routine and simultaneous quantification of TMZ[14,18,58–60].

## Encapsulation efficiency

The encapsulation efficiency (EE%) results demonstrated a statistically significant difference ($p < 0.05$) between the two TMZ-loaded PLGA NP systems prepared using different techniques. The NP1-TMZ formulation, developed via the nanoprecipitation method, exhibited a superior EE of 70.02 ± 2.6%, while the NP2-TMZ system, prepared using the double emulsion solvent evaporation technique, achieved a comparatively lower EE of 54.63 ± 3.1%. This notable disparity can be rationalized based on both the physicochemical properties of TMZ and the fundamental characteristics of the respective formulation techniques.

Nanoprecipitation is a widely utilized, single-step technique that involves the rapid addition of a polymer–drug solution, dissolved in an organic solvent, into an aqueous phase under controlled mixing conditions. This results in immediate solvent exchange and polymer precipitation, forming NPs almost instantaneously. For TMZ, a compound with moderate hydrophobicity and good solubility in various organic solvents such as DMSO, ethanol, and acetone, this method offers a particularly favorable environment for encapsulation. The brief and limited exposure of TMZ to the aqueous phase during nanoprecipitation is especially critical, as the drug is known to undergo rapid hydrolytic degradation under physiological or slightly basic pH conditions. This degradation leads to the formation of inactive byproducts such as MTIC and AIC, thereby reducing the effective drug load. By minimizing the duration of aqueous exposure, nanoprecipitation helps preserve the chemical integrity of TMZ and enhances its entrapment within the polymer matrix. Additionally, the fast solidification kinetics associated with this technique favor efficient molecular entrapment of the drug before it can diffuse into the surrounding medium. In contrast, the double emulsion solvent evaporation (DESE) method is a multi-

step process that begins with the dissolution of TMZ in an internal aqueous phase, which is emulsified into a polymer-containing organic phase to form a primary water-in-oil ($W_1/O$) emulsion. This is subsequently emulsified into an external aqueous phase to generate the final $W_1/O/W_2$ emulsion. During this sequence, TMZ is subjected to prolonged contact with aqueous environments at physiological pH, greatly increasing the potential for degradation. Moreover, the slower kinetics of polymer solidification allow ample time for TMZ to diffuse out of the inner phase into the external aqueous medium, resulting in significant drug loss. These combined factors -chemical instability of TMZ in aqueous media, multiple emulsification steps, and extended processing time- substantially reduce the encapsulation efficiency in the DESE-prepared NP2-TMZ formulation compared to that of NP1-TMZ[61–66].

The encapsulation efficiencies obtained for NP1-TMZ (70.02%) and NP2-TMZ (54.63%) are within the range considered acceptable for oral drug delivery systems[40,67,68]. While the higher EE of NP1-TMZ supports its suitability for oral administration, especially in dose-critical chemotherapeutic regimens, the moderate EE of NP2-TMZ may require further formulation optimization to ensure adequate drug loading and therapeutic consistency.

## In vitro release

In vitro release studies revealed a distinctly different release profile between the two NP formulations of TMZ, as shown in Figs. 5 and 6. The NP1-TMZ system, prepared by the nanoprecipitation method, exhibited a biphasic release pattern characterized by an initial burst release (~30.6% at 1 h), followed by a sustained release phase that extended to ~90.9% at 72 h. This release behavior is consistent with the characteristics of nanoprecipitated systems, where drug molecules located near or on the particle surface are rapidly released, while those entrapped within the polymer matrix undergo diffusion-controlled release over time. In contrast, the NP2-TMZ formulation, developed using the double emulsion-solvent evaporation technique, demonstrated a more gradual and controlled release profile. The initial burst was significantly lower (~14.9% at 1 h), and the cumulative release reached ~86.6% at 72 h. This difference likely stems from the inner aqueous phase used in the double emulsion method, where TMZ is more deeply embedded within the PLGA core. As a result, the drug experiences a more pronounced diffusional barrier, leading to slower release kinetics[69–73].

The release from both NP systems was substantially prolonged in comparison to free TMZ, which exhibited an immediate release of >95% within the first hour under the same test conditions, highlighting the protective and modulating role of PLGA encapsulation. The more rapid release observed in NP1-TMZ may be beneficial in cases where prompt therapeutic exposure is desired, such as initial tumor debulking or induction regimens. On the other hand, the controlled and sustained profile of NP2-TMZ may be more appropriate for maintaining therapeutic plasma concentrations over exten ded periods, thus minimizing dosing frequency and potentially improving patient compliance[1,74–76].

These distinctions underscore the importance of aligning release kinetics with clinical objectives when designing nanoparticulate delivery systems. The comparative release data presented in Fig. 4 (72-hour cumulative release) and Fig. 5 (24-hour release dynamics) clearly support the rational selection of formulation strategy based on the desired temporal drug exposure profile.

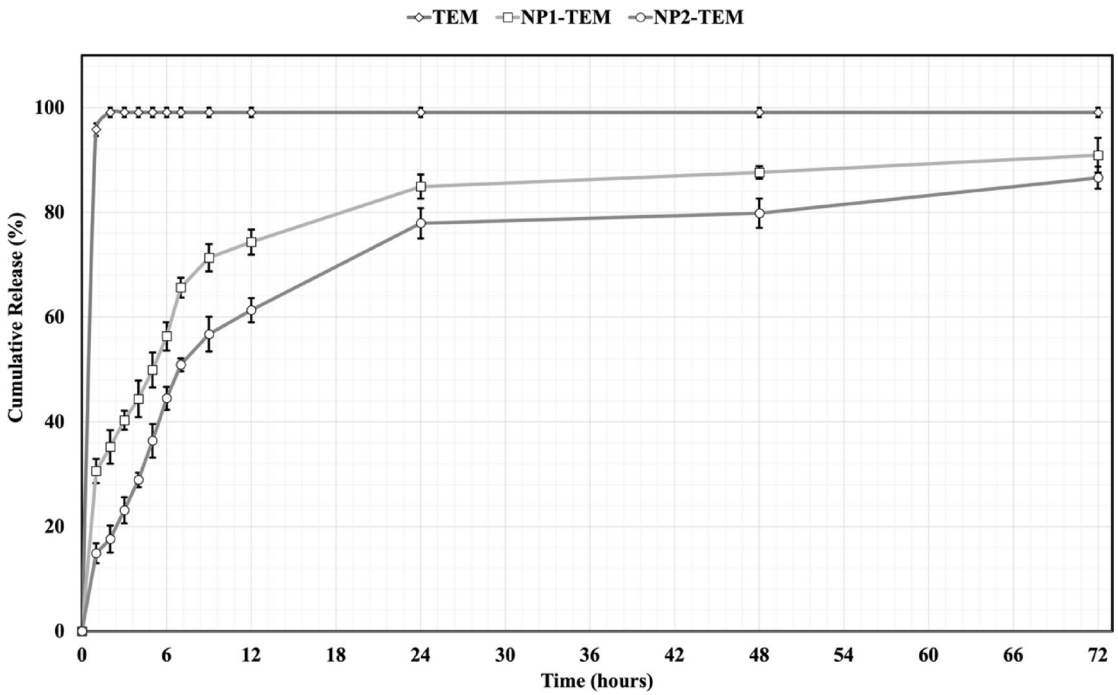



**Fig. 5**. 72-h cumulative release graph for TMZ, NP1-TMZ, and NP2-TMZ.

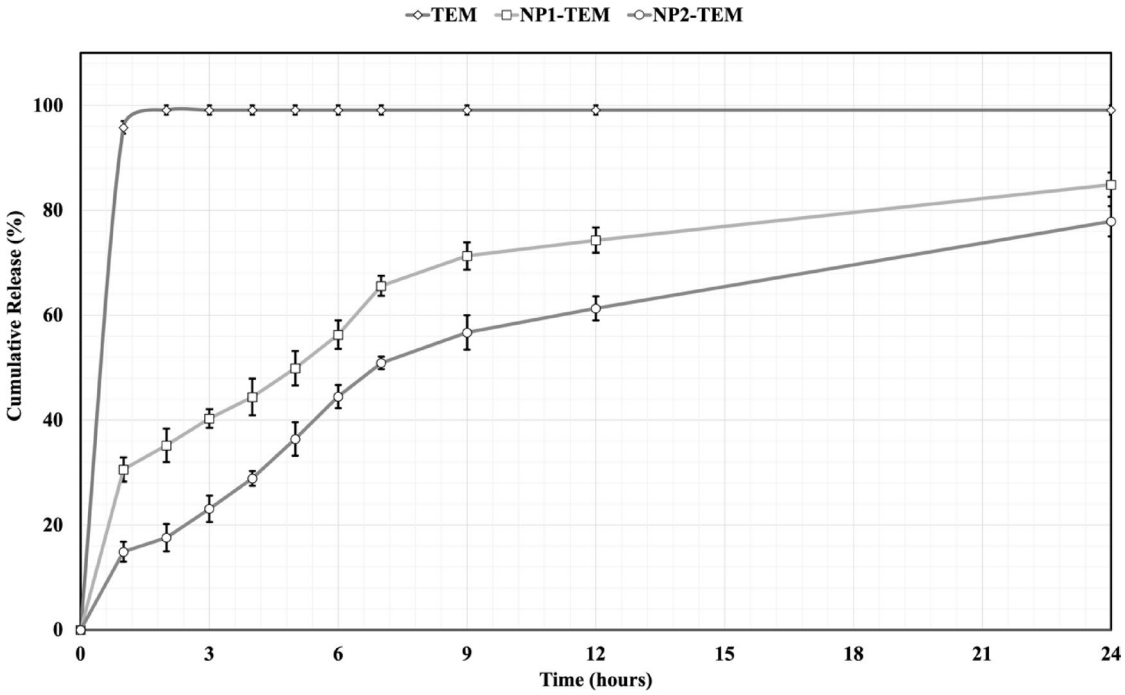



**Fig. 6**. 24-h cumulative release graph for TMZ, NP1-TMZ, and NP2-TMZ.

## Release kinetics

In vitro release data were fitted to various kinetic models including Korsmeyer–Peppas, Higuchi, and Weibull using DDSolver to better understand the drug release mechanisms from the developed NP formulations (See Table 4; Fig. 7). Among the tested models, the Korsmeyer–Peppas equation provided the best fit for both NP1-TMZ and NP2-TMZ, as indicated by the highest coefficient of determination ($R^2$ = 0.989 for NP1-TMZ and 0.977 for NP2-TMZ), along with the lowest AIC and WSS values. The *n* value for NP1-TMZ was 0.331, indicating a Fickian diffusion-controlled release, while NP2-TMZ exhibited a higher *n* value of 0.668, suggesting a non-Fickian (anomalous) transport mechanism, where both diffusion and polymer relaxation contribute to the release process. This result is in agreement with the observed release profiles, where NP1-TMZ showed a prominent initial burst followed by sustained release, whereas NP2-TMZ exhibited a more controlled and gradual profile[77].

The Higuchi model demonstrated a strong linear correlation for NP2-TMZ ($R^2$ = 0.959), suggesting that drug release from this system was predominantly governed by diffusion through the hydrated polymer matrix. In contrast, the Higuchi model showed relatively poor correlation for NP1-TMZ ($R^2$ = 0.884), likely due to the influence of burst release behavior which deviates from the assumptions of a diffusion-limited system[78].

The Weibull model, known for its flexibility in describing complex release mechanisms, also showed a reasonably good fit for both formulations ($R^2$ = 0.966 for NP1-TMZ and 0.958 for NP2-TMZ). The shape parameter $\beta$was less than 1 in both cases ($\beta = 0.450$ for NP1-TMZ and $\beta = 0.594$ for NP2-TMZ), indicating parabolic release kinetics consistent with a diffusion-controlled mechanism. The α values for NP1-TMZ and NP2-TMZ were 2.544 and 5.293, respectively, indicating a slower release onset in the NP2 system. However, the slightly higher AIC and lower MSC values compared to the Peppas model suggested a less optimal fit[79].

The Mean Squared Error (MSE) and Root Mean Squared Error (MSE_root), which reflect the average deviation between experimental and predicted values, were lowest for the Korsmeyer–Peppas model in both formulations, indicating minimal prediction error. The MSE values were 4.516 (NP1-TMZ) and 9.088 (NP2-TMZ), which support the model's statistical accuracy. Moreover, the Sum of Squares (SS) and Weighted Sum of Squares (WSS) were markedly higher in the Higuchi and Weibull models for both NP1-TMZ and NP2-TMZ. This suggests a greater residual error in these models compared to the Peppas model. Similarly, Model Selection Criterion (MSC) values, which combine model complexity and fit quality, were highest for the Peppas model in both formulations (2.822 and 2.904, respectively), further reinforcing its preference as the most suitable kinetic model. The Akaike Information Criterion (AIC) values—used for model comparison—were lowest in the Korsmeyer–Peppas model for NP1-TMZ (25.819) and NP2-TMZ (41.376), which supports the model's parsimony and goodness-of-fit balance. The Weighting factor remained constant (1.000) across all models and formulations, confirming that the data were treated uniformly and that no external bias was introduced in curve fitting. Regarding the Weibull model, additional insights can be gained from the α (scale) and β (shape) parameters. Finally, the Ti (lag time) parameter was 0.400 for both NP1-TMZ and NP2-TMZ in the Weibull model, indicating a short but notable delay before the onset of drug release. This lag phase may be attributed to the time required for hydration and polymer matrix swelling before the initial diffusion of TMZ.

| Parameter | Model and equation | | | | | |
|---|---|---|---|---|---|---|
| | Korsmeyer-Peppas $F = k_{KP}.t^n$ | | Higuchi $F = k_{H^*}.(t)^{0.5}$ | | Weibull $F = 100.\{1\text{-}Exp[-((t\text{-}Ti)^{\beta})/\alpha]\}$ | |
| | NP1-TMZ | NP2-TMZ | NP1-TMZ | NP2-TMZ | NP1-TMZ | NP2-TMZ |
| N_observed | 7.000 | 9.000 | 11.000 | 11.000 | 13.000 | 13.000 |
| DF | 5.000 | 7.000 | 10.000 | 10.000 | 10.000 | 10.000 |
| R_obs-pre | 0.994 | 0.990 | 0.964 | 0.980 | 0.986 | 0.983 |
| Rsqr ($R^2$) | 0.989 | 0.977 | 0.884 | 0.959 | 0.972 | 0.965 |
| Rsqr_adj ($R^2_{adjusted}$) | 0.987 | 0.973 | 0.884 | 0.959 | 0.966 | 0.958 |
| MSE | 4.516 | 9.088 | 66.760 | 22.251 | 23.443 | 31.030 |
| MSE_root | 2.125 | 3.015 | 8.171 | 4.717 | 4.842 | 5.570 |
| Weighting | 1.000 | 1.000 | 1.000 | 1.000 | 1.000 | 1.000 |
| SS | 22.578 | 63.615 | 667.601 | 222.507 | 234.427 | 310.304 |
| WSS | 22.578 | 63.615 | 667.601 | 222.507 | 234.427 | 310.304 |
| AIC | 25.819 | 41.376 | 73.541 | 61.455 | 76.943 | 80.588 |
| MSC | 2.822 | 2.904 | 1.398 | 2.704 | 2.634 | 2.651 |
| kKP | 29.151 | 12.598 | – | – | – | – |
| ***n*** | 0.331 | 0.668 | – | - | – | – |
| kH | – | – | 21.222 | 16.805 | – | – |
| ***α*** | – | – | – | – | 2.544 | 5.293 |
| ***β*** | – | – | – | – | 0.450 | 0.594 |
| Ti | – | – | – | – | 0.400 | 0.400 |

**Table 4**. Kinetic modeling of TMZ release from nanoparticles. *To comprehensively evaluate and compare the release kinetics of NP1-TMZ and NP2-TMZ formulations, three widely accepted mathematical models—Korsmeyer–Peppas, Higuchi, and Weibull—were applied, and key statistical parameters were analyzed. The number of observed data points (N_observed) and degrees of freedom (DF) reflect the dataset size and the model's complexity. The R_obs-pre (correlation between observed and predicted values), $R^2$ (Rsqr), and $R^2_{adjusted}$ (adjusted R-squared) values provide insights into the model fit quality, with higher values indicating better conformity. The MSE (mean square error) and MSE_root (root mean square error) quantify the average prediction error. Weighting refers to the uniform weight given to each data point. SS (sum of squares) and WSS (weighted sum of squares) describe the total residual variability. AIC (Akaike Information Criterion) and MSC (Model Selection Criterion) help in model comparison, with lower AIC and higher MSC values signifying superior model performance. For the Korsmeyer–Peppas model, kKP is the kinetic constant, and ***n*** is the release exponent that helps identify the release mechanism (e.g., $n < 0.5$ indicates Fickian diffusion). In the Higuchi model, kH represents the diffusion rate constant. For the Weibull model, α is the scale parameter indicating the time scale of release, ***β*** is the shape parameter describing the release mechanism ($\beta < 1$ = parabolic, $\beta = 1$ = exponential, $\beta > 1$ = sigmoidal), and Ti denotes the lag time, representing the delay before the onset of drug release. Taken together, these parameters provide a rigorous statistical and mechanistic interpretation of the drug release profiles and support the selection of the most appropriate model for each formulation.

Taken together, these kinetic findings reinforce that the release of TMZ from NP1-TMZ is predominantly driven by Fickian diffusion with significant surface-associated drug, while NP2-TMZ exhibits a more matrix-integrated, sustained release behavior. The results further confirm that formulation method strongly influences the release kinetics, which can be tailored according to therapeutic needs—such as rapid drug availability versus prolonged plasma exposure[29,30].

Similarity analysis (See Table 5) between the two nanoparticulate formulations was conducted using the model-independent similarity factor ($f_2$) supported by bootstrap resampling ($n = 5000$). The observed $f_2$ value between NP1-TMZ and NP2-TMZ was calculated to be 44.52, which falls below the critical threshold of 50, indicating non-similarity between the two dissolution profiles (Tabl. Furthermore, the 5th and 95th percentile values from the bootstrap distribution were identical (44.52), confirming the statistical robustness and consistency of the result. The skewness and kurtosis values (1.000 and – 2.001, respectively) suggested a narrow and slightly skewed distribution. Collectively, these data demonstrate that the drug release behavior of NP1-TMZ and NP2-TMZ differs significantly, further supporting the conclusion that formulation technique plays a crucial role in modulating release kinetics[80].

## Solid-state characterization

*Thermal analysis*

The DSC thermogram of TMZ, Blank NPs and drug-loaded NPs are displayed in Fig. 8. The DSC thermogram of pure TMZ (Fig. 8A) exhibited a sharp endothermic peak at 203.08 °C, corresponding to its melting point,

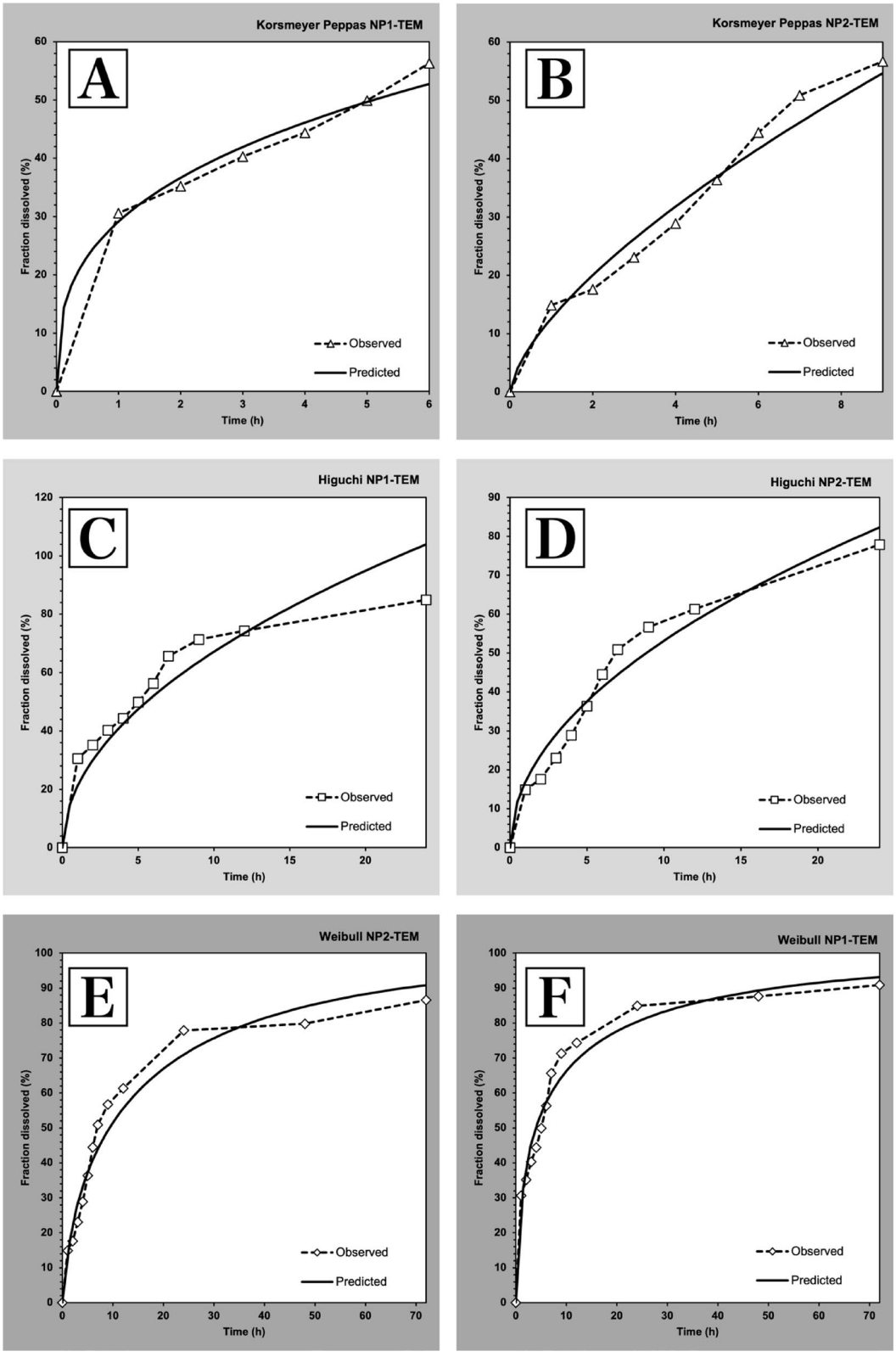



**Fig. 7**. DDSolver program graphs of kinetic modeling of TMZ release from nanoparticles. **A** Korsmeyer–Peppas model for NP1-TMZ; **B** Korsmeyer–Peppas model for NP2-TMZ;**C** Higuchi model for NP1-TMZ; **D** Higuchi model for NP2-TMZ; **E** Weibull model for NP2-TMZ; **F** Weibull model for NP1-TMZ.

| Statistics | Value |
|---|---|
| Observed f2 | 44.520 |
| Number of bootstrap | 5000.000 |
| Bootstrap mean | 44.520 |
| Bootstrap median | 44.520 |
| 5% percentile | 44.520 |
| 95% percentile | 44.520 |
| Skewness | 1.000 |
| Kurtosis | −2.001 |
| Is 5% percentile ¡İ 50 | No |
| Similarity of NP1-TMZ and NP2-TMZ | Reject |

**Table 5**. Bootstrap-based similarity factor ($f_2$) analysis between NP1-TMZ and NP2-TMZ formulations.

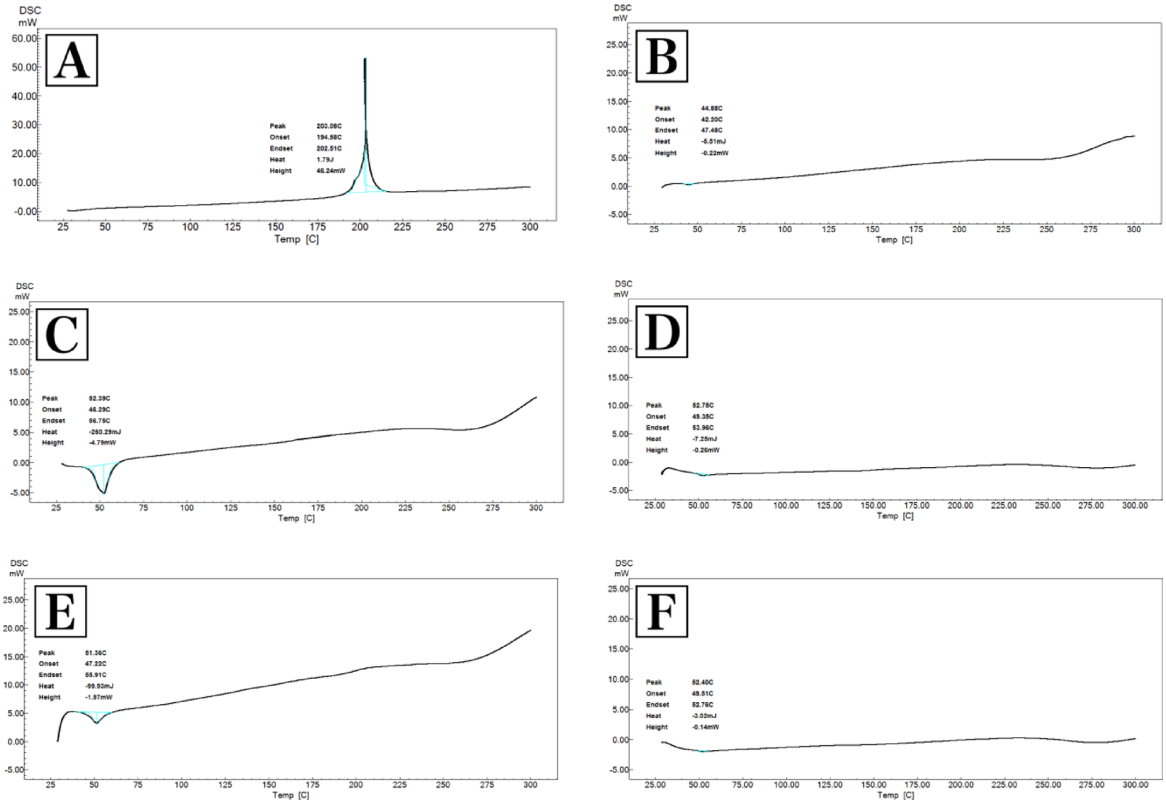



**Fig. 8**. DSC thermograms of TMZ (**A**), PLGA (**B**), NP1-Blank (**C**), NP1-TMZ (**D**), NP2-Blank (**E**), and NP2-TMZ (**F**).

confirming its crystalline nature[81,82]. In contrast, PLGA (Fig. 8B) displayed a glass transition temperature (Tg) around 44.88 °C, as expected for an amorphous polymer[81]. The thermograms of NP1-Blank (Fig. 8C) and NP2-Blank (Fig. 8E) also showed Tg transitions at 52.29 °C and 59.36 °C, respectively, with no melting peaks, indicating the preservation of the amorphous nature of PLGA after NP formation. DSC thermograms of TEM-loaded NPs were similar to Blank NPs. Importantly, the characteristic melting peak of TMZ was absent in both NP1-TMZ (Fig. 8D) and NP2-TMZ (Fig. 8F) thermograms, suggesting that the drug was present in an amorphous or molecularly dispersed state within the polymer matrix[82]. Furthermore, the observed Tg values increased slightly in the drug-loaded formulations, especially in NP1-TMZ, which may indicate stronger drug–polymer interactions and enhanced miscibility in the nanoprecipitation-based formulation.

*Fourier-transform infrared spectroscopy (FTIR) analysis*

The FTIR spectra of TMZ, PLGA, and the developed NP formulations are presented in Fig. 9. In the spectrum of pure TMZ (Fig. 9A), a peak at 1587.42 $cm^{-1}$ is assigned to ν(C = O) (amide carbonyl), while the peaks at 1456.26 $cm^{-1}$ and 1303.88 $cm^{-1}$ are attributed to δ(C–N) and ν(C–C) stretching vibrations of the aromatic and heterocyclic rings. Additionally, the bands observed at 812.03, 734.88, and 657.73 $cm^{-1}$ are indicative of

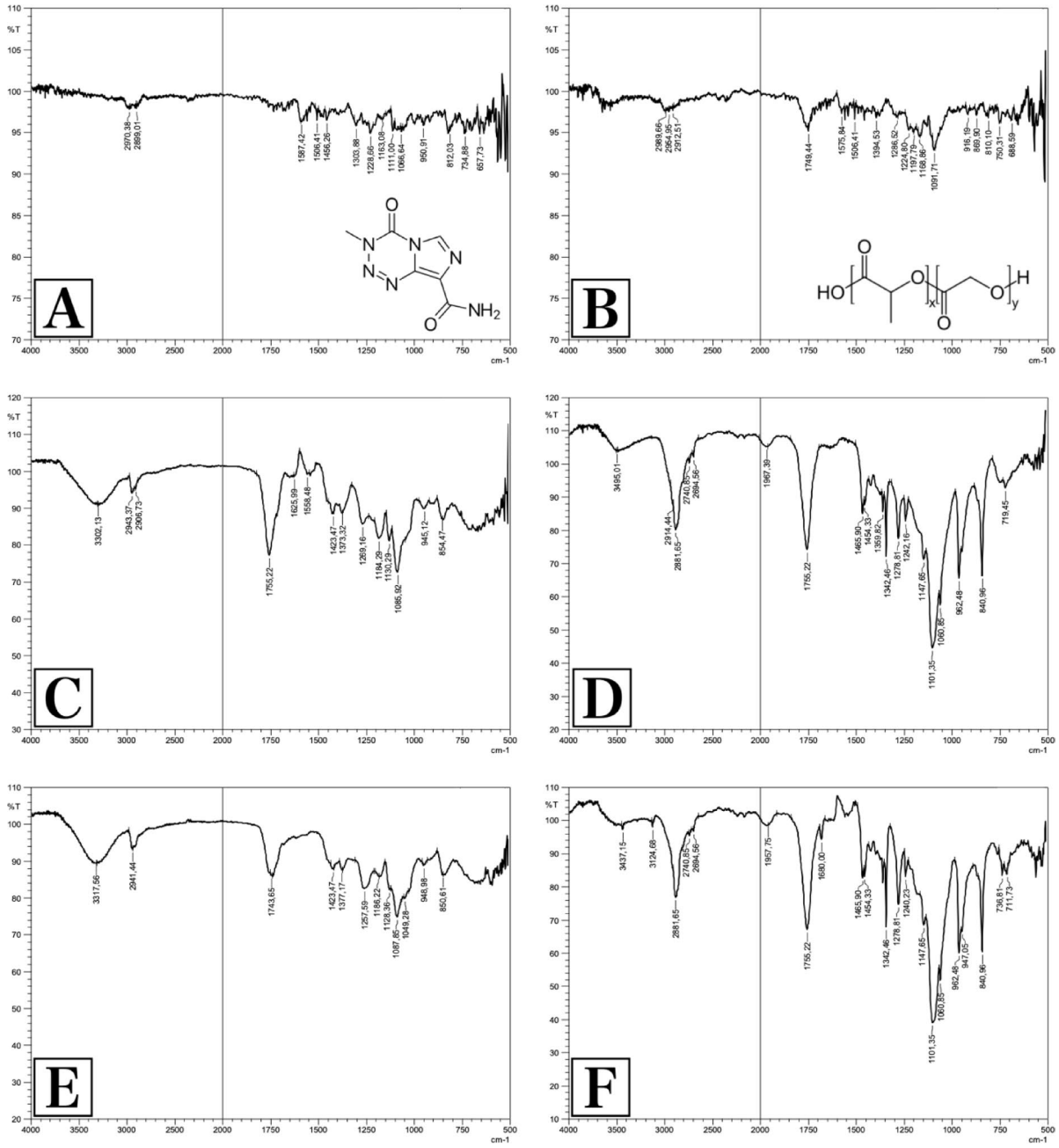



**Fig. 9**. FT-IR spectrums of TMZ (**A**), PLGA (**B**), NP1-Blank (**C**), NP1-TMZ (**D**), NP2-Blank (**E**), and NP2-TMZ (**F**).

γ(C–H) out-of-plane bending modes, confirming the presence of an aromatic system. These findings are in good agreement with the previously reported FTIR data for TMZ[83]. The PLGA spectrum (Fig. 9B) exhibited characteristic ester functionality, with a sharp and intense peak at 1749.44 $cm^{-1}$ corresponding to ν(C = O) (ester carbonyl), and bands in the region of 1091.71 $cm^{-1}$ associated with ν(C–O–C)stretching vibrations. The peaks at 2989.66 $cm^{-1}$ and 2954.95 $cm^{-1}$ were assigned to $\nu(CH_3)$ and $\nu(CH_2)$ stretching of the polymer backbone[84]. The spectrum of the blank NPs prepared via nanoprecipitation (NP1-Blank, Fig. 9C) closely resembled that of PLGA, retaining the dominant ν(C = O) band at 1755.22 $cm^{-1}$ and strong ν(C–O–C) peaks. Similarly, the NP2-Blank formulation (Fig. 9E) showed a spectrum nearly identical to PLGA. NP1-TMZ formulation (Fig. 8D) displayed a broader ν(N–H) band centered at 3495.01 $cm^{-1}$ and a shifted ν(C = O) peak at 1755.22 $cm^{-1}$, suggesting possible hydrogen bonding between the TMZ amide group and the PLGA matrix. The NP2-TMZ formulation (Fig. 9F) exhibited a weak ν(N–H) band at 3437.15 $cm^{-1}$. Compared to NP1-TMZ, these changes were less distinct, suggesting a relatively weaker interaction between TMZ and PLGA in the double emuṣsion solvent evaporation-based NPs. Taken together, the FTIR data demonstrate the successful incorporation of TMZ into both NP1 and NP2 systems, with more pronounced spectral shifts and interactions observed in the NP1-TMZ formulation,

likely due to the favorable dispersion and molecular interaction profile afforded by the nanoprecipitation method[85–87].

## Effects of temozolomid-loaded nanoparticles on U-87 MG and NIH/3T3 cell viability

The evaluation of the anti-cancer effects of TMZ-loaded NPs on the U-87 MG glioblastoma cell line was performed using an MTT assay. Concurrently, the samples were assessed for cytotoxic effects on the NIH/3T3 cell line. The selectivity index (SI), indicating the therapeutic efficacy of the drug candidate as an anticancer agent on cancer cells, was calculated by comparing the $IC_{50}$ results of both tests. According to the results at 400, 100, 10, and 1 $\mu g.mL^{-1}$ concentrations of NP1-TMZ, NP2-TMZ, TMZ, NP1-Blank, and NP2-Blank, U-87 MG cell viability decreased by the following percentages at 24 h: 80.66, 68.65, 40.59, and 27.87; 68.41, 46.95, 26.90, and 17.19; 59.23, 38.03, 7.64, and 10.98; 32.64, 27.97, 14.88, and 8.89; 14.59, 9.72, 9.42, and 3.54. Similarly, at 48 h, the reductions were: 88.95, 92.3, 55.68, and 41.09; 83.18, 70.84, 49.28, and 27.81; 75.21, 44.71, 12.31, and 22.27; 42.43, 29.49, 18.32, and 16.8; 18.93, 18.99, 18.79, and 5.98%, respectively (Fig. 10).

In the 24-hour results, NP1-TMZ and NP2-TMZ at concentrations of 400, 100, 10, and 1 $\mu g.mL^{-1}$ induced NIH/3T3 cell viability decreases of 79.98, 65.66, 28.07, and 21.13: 72.96, 48.01, 18.99, and 23.93%, respectively. Similarly, at 48 h, reductions were observed at 88.13, 93.7, 40.72, and 46.15; 79.90, 74.32, 39.51, and 33.31% (Fig. 11). TMZ concentrations of 400 and 100 $\mu g.mL^{-1}$ resulted in a 52.5% and 20.74% decrease in cell viability at 24 h, while 10 and 1 $\mu g.mL^{-1}$ led to an increase by 8.65% and 34.03%, respectively. At 48 h, TMZ concentrations of 400, 100, 10, and 1 $\mu g.mL^{-1}$ decreased cell viability by 74.19, 44.15, 19.5, and 12.48%, respectively. For NP1-

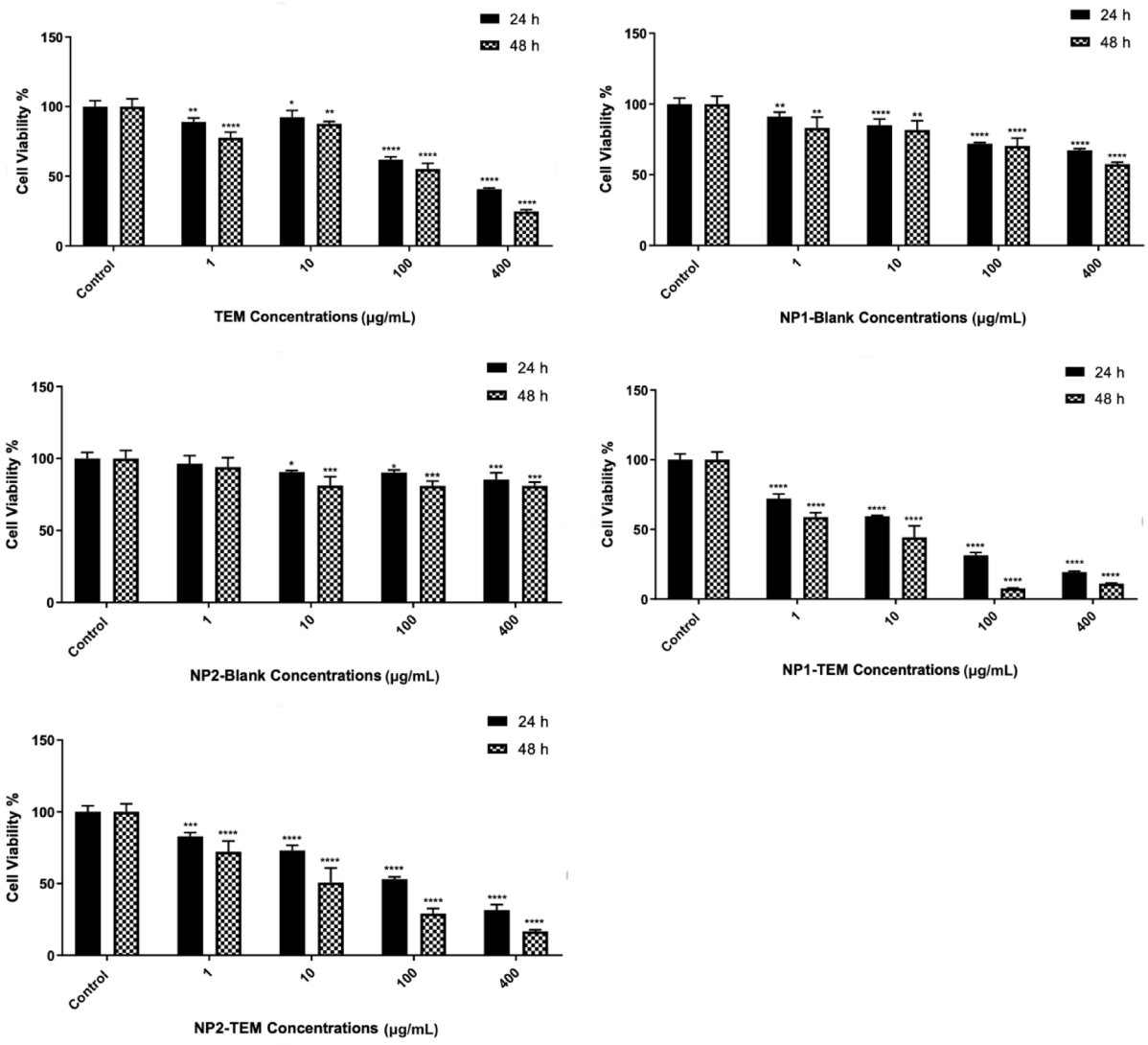



**Fig. 10**. Cell viability assay results for varying concentrations (1, 10, 100, and 400 $\mu g.mL^{-1}$) of TMZ, NP1-TMZ, N2-TMZ, NP1-Blank, and NP2-Blank on U-87 MG cells. Viability was assessed after 24 and 48 h of treatment, and the results are presented as the mean ± SD of three independent experiments (n = 4 for each treatment group). Significant differences are indicated as *$p < 0.05$, **$p < 0.01$, ***$p < 0.001$, ****$p < 0.0001$, while no significant difference is represented as $p > 0.05$ or ns.

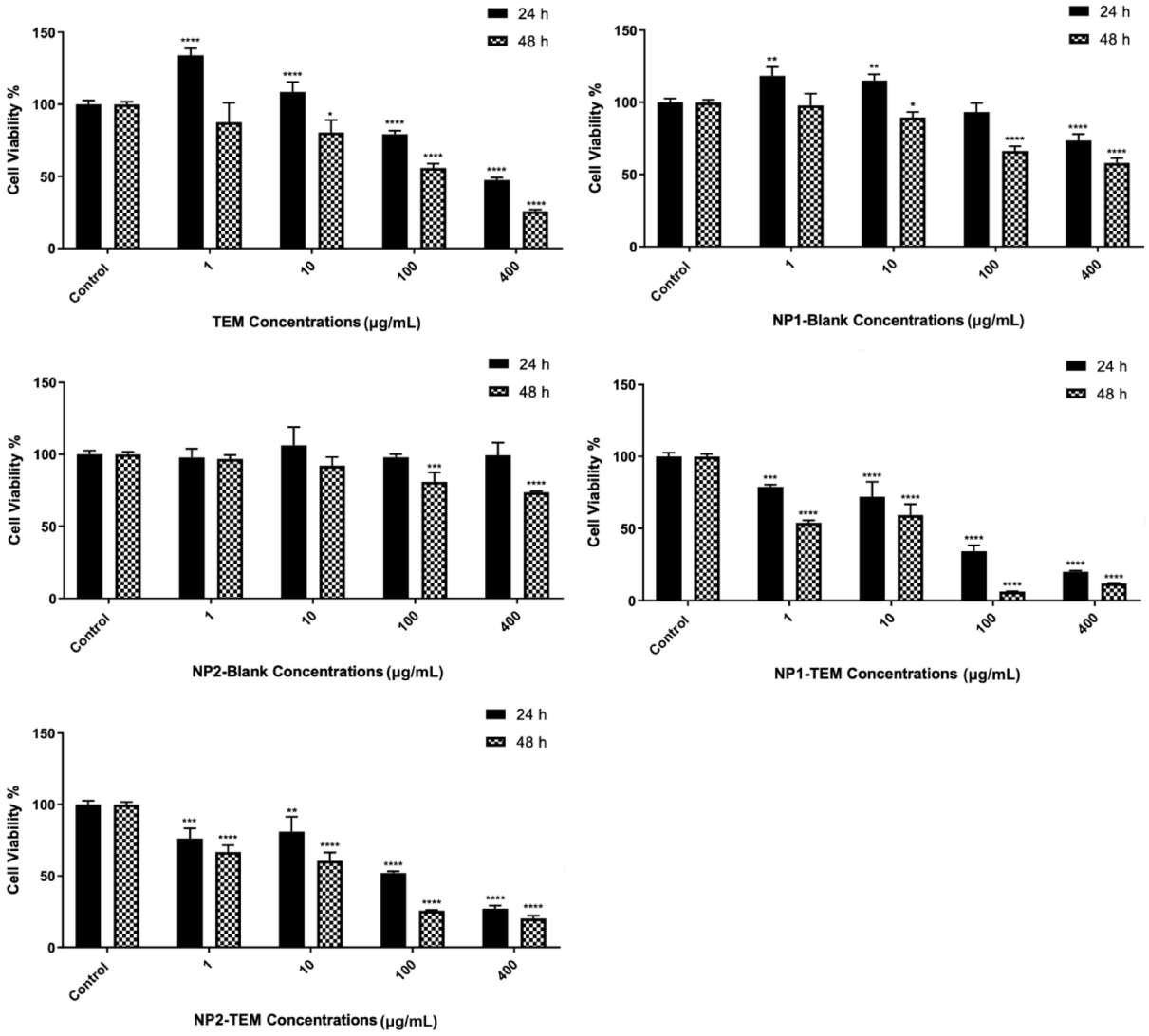



**Fig. 11**. Cell viability assay results for varying concentrations (1, 10, 100, and 400 µg.mL$^{-1}$) of TMZ, NP1-TMZ, N2-TMZ, NP1-Blank, and NP2-Blank on 3T3 cells. Viability was assessed after 24 and 48 h of treatment, and the results are presented as the mean ± SD of three independent experiments (n = 4 for each treatment group). Significant differences are indicated as *p < 0.05, **p < 0.01, ***p < 0.001, ****p < 0.0001, while no significant difference is represented as p > 0.05 or ns.

Blank and NP2-Blank at 24 h, concentrations of 400 and 100 µg.mL$^{-1}$ caused decreases of 29.6% and 6.84%, and 0.56% and 2.11%, while 10 and 1 µg.mL$^{-1}$ led to increases of 15.17, 18.28; 6.2, 2.16%, respectively. At 48 h, NP1 and NP2-Blank at 400, 100, 10, and 1 µg.mL$^{-1}$ resulted in decreases of 41.97, 33.65, 10.57, and 2.04: 26.35, 19.15, 7.81, and 3.17%, respectively.

$IC_{50}$ values for NP1-TMZ, NP2-TMZ, and TMZ on U-87 MG cells were 139.51, 243.04, and 294.43 µg.mL$^{-1}$ at 24 h, and 186.36, 224.29, and 367.76 µg.mL$^{-1}$ at 48 h (Table 6). On NIH/3T3 cells, $IC_{50}$ values for NP1-TMZ, NP2-TMZ, and TMZ were 186.36, 224.29, and 367.76 µg.mL$^{-1}$ at 24 h, and 63.25, 128.78, and 235.87 µg.mL$^{-1}$ at 48 h. NP1-Blank and NP2-Blank exhibited $IC_{50}$ values exceeding 400 µg.mL$^{-1}$ at both 24 and 48 h on both U-87 MG and NIH/3T3 cells.

When the data was collectively evaluated, we determined that NP1-TMZ has a lower $IC_{50}$ value compared to TMZ at both 24 and 48 h, and its selectivity is particularly 2.89-fold higher at 48 h. The lower $IC_{50}$ value suggests a potentially heightened efficacy of NP1-TMZ in inhibiting the growth of U-87 MG cells. Furthermore, the increased selectivity at 48 h emphasizes its potential therapeutic advantage. This data offers insights into the compound's capacity to target specific cells while minimizing the impact on non-cancerous cells, a crucial aspect in the development of anticancer agents.

## Effects of temozolomid-loaded nanoparticles on ROS generation

In an inflammatory milieu, the intense generation of antimicrobial and tumor-killing ROS is referred to as an "oxidative burst," playing a pivotal role as the primary line of defense against environmental pathogens[88].

| | U-87 MG | | NIH/3T3 | | Selectivity index | |
|---|---|---|---|---|---|---|
| | 24 h | 48 h | 24 h | 48 h | 24 h | 48 h |
| TMZ | 294.43 | 187.74 | 367.76 | 235.88 | 1.25 | 1.26 |
| NP1-TMZ | 139.51 | 21.85 | 186.36 | 63.25 | 1.34 | 2.89 |
| NP2-TMZ | 243.04 | 107.00 | 224.29 | 128.78 | 0.92 | 1.20 |
| NP1-Blank | > 400 | > 400 | > 400 | > 400 | – | – |
| NP2-Blank | > 400 | > 400 | > 400 | > 400 | – | – |

**Table 6**. The $IC_{50}$ and SI values for TMZ, NP1/2-TMZ, and NP1/2-Blank obtained from cell viability data.

Recently, there has been notable interest in anticancer treatments that trigger oxidative stress through the elevation of ROS and/or the inhibition of antioxidant mechanisms. The escalation of accumulated ROS disrupts redox homeostasis, leading to severe damage in cancer cells[89].

According to our results, TMZ, NP1-TMZ, and NP2-TMZ increased the production of ROS at all the tested concentrations (Fig. 12). While TMZ led to more significant increases at 100 and 400 $\mu g.mL^{-1}$, NP1-TMZ and NP2-TMZ induced ROS production at 10, 100, and 400 $\mu g.mL^{-1}$. The higher rate of ROS production by NPs at lower concentrations may confer an advantage in causing damage to cancer cells. Additionally, it was observed that the compounds induced ROS formation with a profile similar to their cytotoxic effects on U87-MG cells.

Although this study successfully demonstrated the cytotoxic selectivity and ROS-inducing potential of TMZ-loaded PLGA NPs against glioblastoma cells, we acknowledge that further biological evaluations are required to comprehensively elucidate their intracellular behavior and therapeutic mechanism. In future studies, advanced cellular assays—such as nanoparticle internalization (e.g., fluorescence or confocal microscopy), apoptosis analysis (e.g., Annexin V/PI staining), mitochondrial membrane potential assays (e.g., JC-1 dye), and cell cycle profiling (e.g., flow cytometry)—will be performed to investigate the mechanistic pathways involved in the anti-cancer activity. These extended evaluations will provide deeper insights into the therapeutic potential of the developed nanocarriers and further validate their suitability for brain-targeted chemotherapy[90,91]. While the current study provides an initial in vitro evaluation using cytotoxicity and ROS assays, future work will include advanced cellular studies such as nanoparticle uptake, apoptosis quantification, and mechanistic pathway analysis to further elucidate the anticancer potential of the formulations.

## Conclusion

In this study, TMZ-loaded PLGA nanoparticles were successfully formulated using both nanoprecipitation and double emulsion solvent evaporation methods, enabling a comprehensive comparison of two distinct nanotechnological strategies for oral GBM therapy. The findings revealed that the nanoprecipitation method (NP1-TMZ) provided nanoparticles with smaller size, lower polydispersity, higher encapsulation efficiency, faster drug release, and superior tumor selectivity compared to the double emulsion-derived nanoparticles (NP2-TMZ). Solid-state analyses (DSC and FTIR) confirmed the successful molecular dispersion of TMZ within the polymer matrix without inducing any chemical interactions. Solid-state analyses (DSC and FTIR) confirmed the absence of crystalline TMZ and indicated strong drug–polymer interactions, supporting the integrity of the nanoformulations. Furthermore, biological evaluations highlighted that NP1-TMZ induced a significantly higher generation of reactive oxygen species and exhibited greater cytotoxicity towards U-87 MG glioblastoma cells while maintaining reduced toxicity in NIH/3T3 fibroblast cells, reflecting an enhanced therapeutic index. Collectively, these results underscore the potential of nanoprecipitation-based nanoformulations to overcome the major pharmacokinetic and therapeutic challenges associated with conventional TMZ administration. The innovative approach combining optimized nanoencapsulation, targeted cytotoxicity, and sustained drug release establishes a promising platform for advancing TMZ-based therapies against glioblastoma, potentially improving clinical outcomes for patients afflicted with this devastating malignancy.

Although several studies have investigated TMZ-loaded PLGA nanoparticles, our study provides a comparative analysis of two distinct nanoparticle preparation techniques under identical experimental conditions. The combined evaluation of release kinetics using DDSolver, similarity factor ($f_2$) analysis with bootstrap validation, and ROS-mediated selectivity index offers a unique perspective on formulation-performance relationships for oral TMZ delivery. This integrative approach distinguishes our study from previous reports.

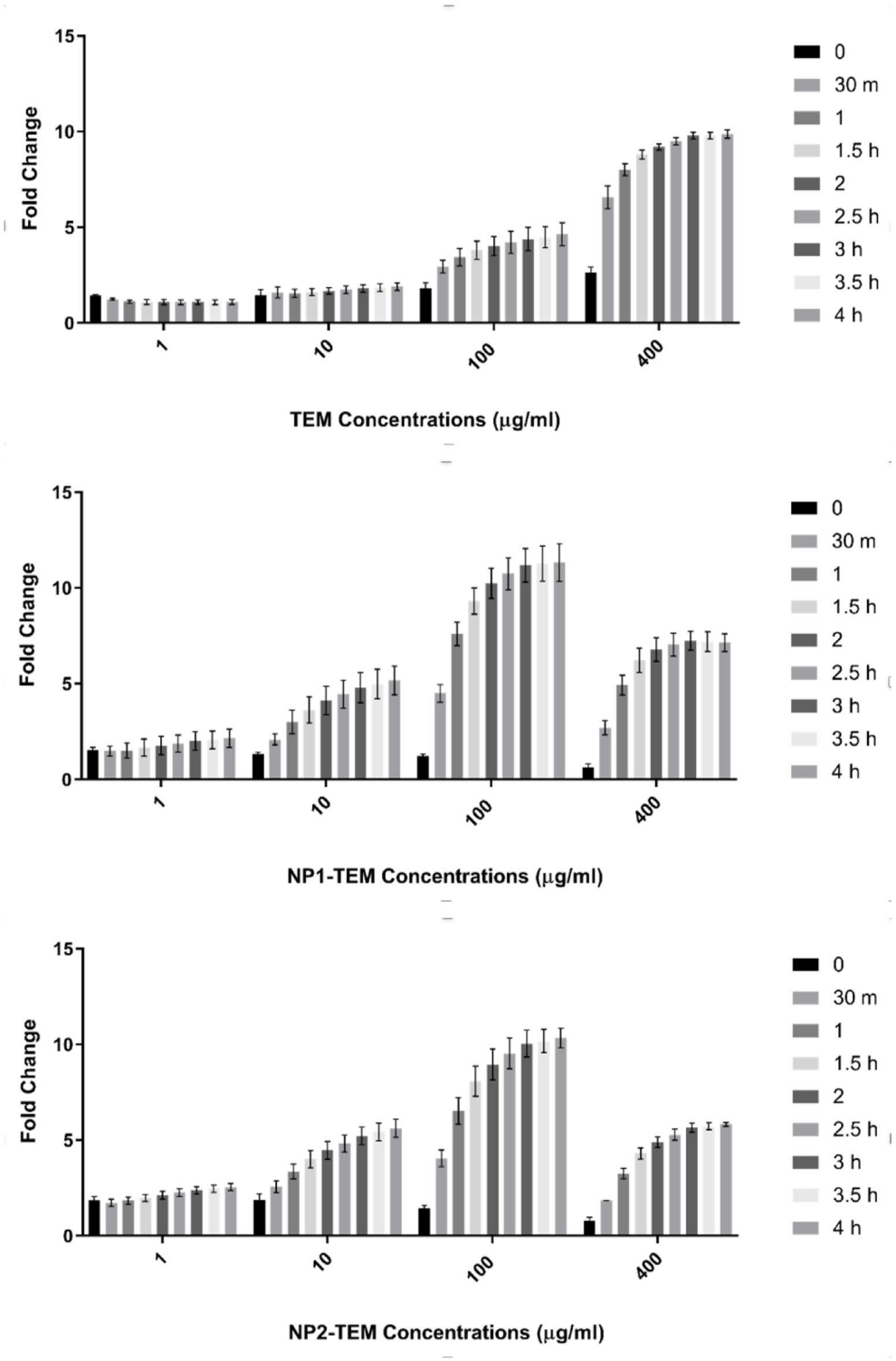



**Fig. 12**. ROS production in U87-MG cells induced by TMZ, NP1-TMZ, and NP2-TMZ.

## Data availability

All results obtained during this study are included in the article, and a supplementary file containing release kinetics, DSC and FTIR analyses is provided to the presented version.

Received: 29 April 2025; Accepted: 11 September 2025
Published online: 16 October 2025

## References


1. Ke, G. et al. Exploratory study on nanoparticle Co-Delivery of Temozolomide and ligustilide for enhanced brain tumor therapy. *Pharmaceutics* **17**, 191 (2025).
2. Ostrom, Q. T. et al. CBTRUS statistical report: primary brain and other central nervous system tumors diagnosed in the united States in 2013–2017. *Neuro Oncol.* **22**, iv1–iv96 (2020).
3. Jezierzański, M. et al. Temozolomide (TMZ) in the treatment of glioblastoma multiforme—A literature review and clinical outcomes. *Curr. Oncol.* **31**, 3994–4002 (2024).
4. Gozdz, A. Proteasome inhibitors against glioblastoma—Overview of molecular mechanisms of cytotoxicity, progress in clinical trials, and perspective for use in personalized medicine. *Curr. Oncol.* **30**, 9676–9688 (2023).
5. Jia, J. L., Alshamsan, B. & Ng, T. L. Temozolomide chronotherapy in glioma: a systematic review. *Curr. Oncol.* **30**, 1893–1902 (2023).
6. Singh, P. et al. Enhancing Temozolomide in vivo stability and efficacy through hybrid nanoconjugate approach for improved glioblastoma multiforme treatment. *Asian J. Pharm. Sci.* **101022** (2025).
7. Jatyan, R. et al. Polymeric and small molecule-conjugates of Temozolomide as improved therapeutic agents for glioblastoma multiforme. *J. Controlled Release*. **350**, 494–513 (2022).
8. Blagosklonny, M. V. Selective protection of normal cells from chemotherapy, while killing drug-resistant cancer cells. *Oncotarget* **14**, 193 (2023).
9. Nordling-David, M. M. et al. Liposomal Temozolomide drug delivery using convection enhanced delivery. *J. Controlled Release*. **261**, 138–146 (2017).
10. Duwa, R. et al. Cetuximab conjugated temozolomide-loaded Poly (lactic-co-glycolic acid) nanoparticles for targeted nanomedicine in EGFR overexpressing cancer cells. *J. Drug Deliv Sci. Technol.* **60**, 101928 (2020).
11. Patil, R. et al. Temozolomide delivery to tumor cells by a multifunctional nano vehicle based on Poly (β-L-malic acid). *Pharm. Res.* **27**, 2317–2329 (2010).
12. Xu, K. et al. Increased the TMZ concentration in brain by Poly (2-ethyl-2-oxazoline) conjugated Temozolomide prodrug micelles for glioblastoma treatment. *Eur. Polym. J.* **145**, 110232 (2021).
13. Xu, Y. et al. The synergic antitumor effects of Paclitaxel and Temozolomide co-loaded in mPEG-PLGA nanoparticles on glioblastoma cells. *Oncotarget* **7**, 20890 (2016).
14. Solak, B., Soyer, P., Tilki, E. K. & Öztürk, A. A. Evaluation of antimicrobial properties and antioxidant activity of Rosmarinic Acid-Loaded resomer RG 502 H-Based nanoparticles against Tert-Butyl Hydroperoxide-Induced oxidative stress: A detailed formulation, characterization and efficacy determination study. *J. Drug Deliv. Sci. Technol.* **106721** (2025).
15. Öztürk, A. A. & Aygül, A. Design of Cefaclor monohydrate containing nanoparticles with extended antibacterial effect by Nano-Spray dryer: A Nanoenglobing study. *J. Res. Pharm.* **24**, 100–111 (2020).
16. Kaya-Tilki, E., Öztürk, A. A., Engür-Öztürk, S. & Dikmen, M. Enhanced anti-angiogenic effects of aprepitant-loaded nanoparticles in human umbilical vein endothelial cells. *Sci. Rep.* **14**, 19837 (2024).
17. Kaval, B., Şen, F. D., Batmaz, K. K., Ekinci, M. & Öztürk, A. A. Latest research about active pharmaceutical ingredient loaded Poly lactic acid-co-Glycolic acid (PLGA) based drug delivery system in Türkiye. *Eur. J. Life Sci.* **1**, 127–139 (2023).
18. Arınmış, K. N., Kıyan, H. T. & Öztürk, A. A. Preparation, characterization, antioxidant activities, and determination of anti-Alzheimer effects of PLGA-based DDSs containing ferulic acid. *ACS Omega*. **9**, 11321–11338 (2024).
19. Baghirova, L., Kaya Tilki, E. & Öztürk, A. A. Evaluation of cell proliferation and wound healing effects of vitamin A Palmitate-Loaded PLGA/Chitosan-Coated PLGA nanoparticles: preparation, characterization, release, and release kinetics. *ACS Omega*. **8**, 2658–2668 (2023).
20. Öztürk, A. A., Namlı, İ. & Aygül, A. Cefaclor Monohydrate-Loaded Colon-Targeted nanoparticles for use in COVID-19 dependent coinfections and intestinal symptoms: formulation, characterization, release kinetics, and antimicrobial activity. *Assay. Drug Dev. Technol.* **19**, 156–175 (2021).
21. Ekinci, M., Öztürk, A. A., Santos-Oliveira, R. & İlem-Özdemir, D. The use of Lamivudine-loaded PLGA nanoparticles in the diagnosis of lung cancer: preparation, characterization, radiolabeling with 99mTc and cell binding. *J. Drug Deliv Sci. Technol.* **69**, 103139 (2022).
22. Öztürk, A. A. & Kırımlıoğlu, G. Y. Preparation and in vitro of characterization lamivudine loaded nanoparticles prepared by acid or ester terminated PLGA for effective oral antiretroviral therapy. *J. Res. Pharm.* **23**, 897–913 (2019).
23. Öztürk, A. A., Çinar, N. İ & Yenilmez, E. Development of nano-sized ketoprofen lysine incorporated Eudragit® S100 nanomedicine by double emulsion solvent evaporation and in vitro characterization. *J. Pharm. Pharmacogn Res.* **7**, 47–58 (2019).
24. Committee, I. C. H. S. ICH Q2B validation of analytical procedures: methodology. *European agency for the evaluation of medicinal products, International commission on harmonisation, London (CPMP/ICH/281/95)* (1996).
25. Guideline, I. C. H. H. Validation of analytical procedures Q2 (R2). *ICH: Geneva, Switzerland* (2022).
26. Borman, P. & Elder, D. Q2 (R1) validation of analytical procedures. *ICH Qual. Guidelines* 127–166 (2017).
27. Öztürk, A. A., Güven, U. M., Yenilmez, E. & Şenel, B. Effects of different derivatives of Eudragit polymer on entrapment efficiency, in vitro dissolution, release kinetics and cell viability results on extended release flurbiprofen loaded nanomedicines. *Lat. Am. J. Pharm.* **37**, 1981–1992 (2018).
28. Öztürk, A. A., Banderas, M., Cayero Otero, L., Yenilmez, M. D., Yazan, Y. & E. & New approach to hypertension treatment: carvediol-loaded PLGA nanoparticles, preparation, in vitro characterization and Gastrointestinal stability. *Lat. Am. J. Pharm.* **37**, 1730–1741 (2018).
29. Zuo, J., Gao, Y., Bou-Chacra, N. & Löbenberg, R. Evaluation of the DDSolver software applications. *Biomed. Res. Int.* **2014**, (2014).
30. Zhang, Y. et al. DDSolver: an add-in program for modeling and comparison of drug dissolution profiles. *AAPS J.* **12**, 263–271 (2010).
31. Öztürk, A. A., Başaran, E., Şenel, B., Demirel, M. & Sarıca, Ş. Synthesis, characterization, antioxidant activity of quercetin, Rutin and Quercetin-Rutin incorporated β-cyclodextrin inclusion complexes and determination of their activity in NIH-3T3, MDA-MB-231 and A549 cell lines. *J. Mol. Struct.* **1282**, 135169 (2023).
32. Öztürk, A. A., Yenilmez, E., Arslan, R., Şenel, B. & Yazan, Y. Dexketoprofen Trometamol loaded solid lipid nanoparticles (SLNs): formulation, in vitro and in vivo evaluation. *J. Res. Pharm.* **24**, 82–99 (2020).
33. Güven, U. M., Öztürk, A. A. & Yenilmez, E. Evaluation of carvedilol-loaded eudragit® nanoparticles. *J. Res. Pharm.* **24**, 71–81 (2020).
34. Haffani, Y. Z. et al. Anti-tumoral activity of allium roseum compounds on breast cancer cells MCF7 and MDA-MB231. *Adv. Traditional Med.* **1–11** (2023).
35. Dikmen, M., Canturk, Z., Tilki, E. K. & Engur, S. Evaluation of antiangiogenic and antimetastatic effects of penicillium chrysogenum secondary metabolites. *Indian J. Pharm. Sci.* **79**, 49–57 (2017).
36. Baghirova, L., Kaya Tilki, E. & Ozturk, A. A. Evaluation of cell proliferation and wound healing effects of vitamin A Palmitate-Loaded PLGA/Chitosan-Coated PLGA nanoparticles: preparation, characterization, release, and release kinetics. *ACS Omega*. **8**, 2658–2668 (2023).
37. Mosmann, T. Rapid colorimetric assay for cellular growth and survival: application to proliferation and cytotoxicity assays. *J. Immunol. Methods*. **65**, 55–63 (1983).
38. Lica, J. J. et al. Effective drug concentration and selectivity depends on fraction of primitive cells. *Int. J. Mol. Sci.* **22**, 4931 (2021).

39. Banerjee, A., Banerjee, V., Czinn, S. & Blanchard, T. Increased reactive oxygen species levels cause ER stress and cytotoxicity in Andrographolide treated colon cancer cells. *Oncotarget* **8**, 26142 (2017).
40. Kömür, M., Kıyan, H. T. & Öztürk, A. A. Development of donepezil hydrochloride-loaded PLGA-based nanoparticles for alzheimer's disease treatment. *Sci. Rep.* **15**, 13184 (2025).
41. Yusuf, A., Almotairy, A. R. Z., Henidi, H., Alshehri, O. Y. & Aldughaim, M. S. Nanoparticles as drug delivery systems: a review of the implication of nanoparticles' physicochemical properties on responses in biological systems. *Polym. (Basel)*. **15**, 1596 (2023).
42. Huang, W., Tsui, C. P., Tang, C. Y. & Gu, L. Effects of compositional tailoring on drug delivery behaviours of silica xerogel/polymer core-shell composite nanoparticles. *Sci. Rep.* **8**, 13002 (2018).
43. Shen, S., Wu, Y., Liu, Y. & Wu, D. High drug-loading nanomedicines: progress, current status, and prospects. *Int. J. Nanomedicine* 4085–4109 (2017).
44. Di Filippo, L. D., Duarte, J. L., Luiz, M. T., de Araújo, J. T. C. & Chorilli, M. Drug delivery nanosystems in glioblastoma multiforme treatment: current state of the Art. *Curr. Neuropharmacol.* **19**, 787–812 (2021).
45. Ramalho, M. J. et al. Receptor-mediated PLGA nanoparticles for glioblastoma multiforme treatment. *Int. J. Pharm.* **545**, 84–92 (2018).
46. Kurban, B. et al. Elemi essential oil nanocapsulated drug ameliorates lung cancer via oxidative stress, apoptosis and inflammation pathway. *J. Cell. Mol. Med.* **27**, 1887–1899 (2023).
47. Ekinci, M., Öztürk, A. A. & İlem özdemir, D. Preparation, radiolabeling and cell culture studies of Chitosan coated PLGA nanoparticles as a potential cancer diagnostic agent. *J. Res. Pharmacy* **26**, (2022).
48. Öztürk, A. A., Tilki, E. K., Güven, U. M. & Kıyan, H. T. Ketorolac tromethamine loaded Nano-Spray dried nanoparticles: preparation, characterization, cell viability, COL1A1 gene simulation and determination of Anti-inflammatory activity by in vivo HET-CAM assay. *Curr. Drug Deliv.* **20**, 830–840 (2023).
49. Elmaskaya, A., Öztürk, A. A., Büyükköroğlu, G. & Yenilmez, E. Spray-dried ketoprofen lysine-incorporated PLGA nanoparticles; formulation, characterization, evaluation and cytotoxic profile. *Indian J. Pharm. Sci.* **81**, (2019).
50. Öztürk, A. A., Ünver, H. & Kıyan, H. T. Antioxidant and antiangiogenic effect of homoleptic palladium (II) Car-boxamide complex loaded Chitosan modified PLGA nanoparticles: in vitro evaluation and in vivo chick embryo Chorioallantoic membrane (CAM) assay. *Lett. Drug Des. Discov.* **20**, 1158–1170 (2023).
51. Chigumira, W. et al. Preparation and evaluation of pralidoxime-loaded PLGA nanoparticles as potential carriers of the drug across the blood brain barrier. *J. Nanomater* **2015**, 692672 (2015).
52. Quaglia, F. et al. The intracellular effects of non-ionic amphiphilic cyclodextrin nanoparticles in the delivery of anticancer drugs. *Biomaterials* **30**, 374–382 (2009).
53. Honary, S. & Zahir, F. Effect of zeta potential on the properties of nano-drug delivery systems-a review (Part 2). *Trop. J. Pharm. Res.* **12**, 265–273 (2013).
54. Saraiva, C. et al. Nanoparticle-mediated brain drug delivery: overcoming blood–brain barrier to treat neurodegenerative diseases. *J. Controlled Release*. **235**, 34–47 (2016).
55. Nikandish, N., Hosseinzadeh, L., Azandaryani, A. H. & Derakhshandeh, K. The role of nanoparticle in brain permeability: an in-vitro BBB model. *Iran. J. Pharm. Res.* **15**, 403 (2016).
56. Lockman, P. R., Koziara, J. M., Mumper, R. J. & Allen, D. D. Nanoparticle surface charges alter blood–brain barrier integrity and permeability. *J. Drug Target.* **12**, 635–641 (2004).
57. Wu, D. et al. The blood–brain barrier: structure, regulation and drug delivery. *Signal. Transduct. Target. Ther.* **8**, 217 (2023).
58. Çevikelli, T., Güven, U. M. & Öztürk, A. A. Metronidazole loaded novel microemulsion formulation for topical delivery and characterization with validated new UPLC method. *Fabad J. Pharm. Sci.* **49**, 111–128 (2024).
59. Öztürk, A. A., Güven, U. M. & Yenilmez, E. Flurbiprofen loaded gel based topical delivery system: formulation and in vitro characterization with new developed UPLC method. *ACTA Pharm. Sciencia*. **56**, 81–105 (2018).
60. Öztürk, A. A. & Güven, U. M. Cefaclor monohydrate loaded microemulsion formulation for topical application: characterization with new developed UPLC method and stability study. *J. Res. Pharm.* **23**, 426–440 (2019).
61. Salatin, S. et al. Development of a nanoprecipitation method for the entrapment of a very water soluble drug into Eudragit RL nanoparticles. *Res. Pharm. Sci.* **12**, 1–14 (2017).
62. Bovone, G., Cousin, L., Steiner, F. & Tibbitt, M. W. Solvent controls nanoparticle size during nanoprecipitation by limiting block copolymer assembly. *Macromolecules* **55**, 8040–8048 (2022).
63. Hou, X. et al. Core-shell type thermo-nanoparticles loaded with Temozolomide combined with photothermal therapy in melanoma cells. *Oncol. Rep.* **42**, 2512–2520 (2019).
64. Rodriguez de Anda, D. A., Ohannesian, N., Martirosyan, K. S. & Chew, S. A. Effects of solvent used for fabrication on drug loading and release kinetics of electrosprayed temozolomide-loaded PLGA microparticles for the treatment of glioblastoma. *J. Biomed. Mater. Res. B Appl. Biomater.* **107**, 2317–2324 (2019).
65. Krajcer, A., Grzywna, E. & Lewandowska-Łańcucka, J. Strategies increasing the effectiveness of Temozolomide at various levels of anti-GBL therapy. *Biomed. Pharmacother.* **165**, 115174 (2023).
66. Iturrioz-Rodríguez, N., Sampron, N. & Matheu, A. Current advances in Temozolomide encapsulation for the enhancement of glioblastoma treatment. *Theranostics* **13**, 2734 (2023).
67. Panyam, J., Williams, D., Dash, A., Leslie-Pelecky, D. & Labhasetwar, V. Solid-state solubility influences encapsulation and release of hydrophobic drugs from PLGA/PLA nanoparticles. *J. Pharm. Sci.* **93**, 1804–1814 (2004).
68. Martín-Banderas, L. et al. Cannabinoid derivate-loaded PLGA nanocarriers for oral administration: formulation, characterization, and cytotoxicity studies. *Int. J. Nanomed.* **7**, 5793 (2012).
69. Jain, D. S. et al. Unraveling the cytotoxic potential of Temozolomide loaded into PLGA nanoparticles. *DARU J. Pharm. Sci.* **22**, 1–9 (2014).
70. Lee, C. Y. Strategies of Temozolomide in future glioblastoma treatment. *Onco. Targets Ther.* 265–270 (2017).
71. Fang, C. et al. Temozolomide nanoparticles for targeted glioblastoma therapy. *ACS Appl. Mater. Interfaces*. **7**, 6674–6682 (2015).
72. Ling, Y., Wei, K., Zou, F. & Zhong, S. Temozolomide loaded PLGA-based superparamagnetic nanoparticles for magnetic resonance imaging and treatment of malignant glioma. *Int. J. Pharm.* **430**, 266–275 (2012).
73. Bernal, G. M. et al. Convection-enhanced delivery and in vivo imaging of polymeric nanoparticles for the treatment of malignant glioma. *Nanomedicine* **10**, 149–157 (2014).
74. Remco, L. *Nanocarrier drug-delivery systems for temozolomide in the treatment of glioblastoma multiforme* (Rijksuniversiteit Groningen, 2021).
75. Ananta, J. S., Paulmurugan, R. & Massoud, T. F. Temozolomide-loaded PLGA nanoparticles to treat glioblastoma cells: a biophysical and cell culture evaluation. *Neurol. Res.* **38**, 51–59 (2016).
76. Erthal, L. C. S., Shi, Y., Sweeney, K. J., Gobbo, O. L. & Ruiz-Hernandez, E. Nanocomposite formulation for a sustained release of free drug and drug-loaded responsive nanoparticles: an approach for a local therapy of glioblastoma multiforme. *Sci. Rep.* **13**, 5094 (2023).
77. Ismailovi, N., Kıyan, H. T. & Öztürk, A. A. A novel phytotherapy application: preparation, characterization, Antiox-idant activities and determination of Anti-inflammatory effects by in vivo HET-CAM assay of Chitosan-based DDSs containing endemic Helichry-sum pamphylicum PH Davis & Kupicha methanolic extract. *Curr. Drug Deliv.* (2023).
78. Polat, G., Koçum, İ. C. & Açıkel, Y. S. Development of a magnetic field-triggered system with magnetic silica nanoparticles for enhanced controlled protein release. *J. Magn. Magn. Mater.* **624**, 173059 (2025).

79. Öztürk, A. A., Namlı, İ., Güleç, K. & Görgülü, Ş. Design of lamivudine loaded nanoparticles for oral application by nano spray drying method: a new approach to use an antiretroviral drug for lung cancer treatment. *Comb. Chem. High. Throughput Screen.* **23**, 1064–1079 (2020).
80. Jamil, R. & Polli, J. E. Application of bootstrap f to dissolution data from biorelevant media and evidence of the Conservative nature of bootstrap f. *Eur. J. Pharm. Sci.* **196**, 106745 (2024).
81. Zhang, H. & Gao, S. Temozolomide/PLGA microparticles and antitumor activity against glioma C6 cancer cells in vitro. *Int. J. Pharm.* **329**, 122–128 (2007).
82. Kouhjani, M., Jaafari, M. R., Saberi, A., Gholami, L. & Tafaghodi, M. Nose to brain delivery of insulin loaded in PLGA and chitosan-coated PLGA nanoparticles: A promising approach for alzheimer's disease therapy. *J. Drug Deliv Sci. Technol.* **108**, 106857 (2025).
83. Bhat, S. A. & Ahmad, S. Quantum chemical calculations and analysis of FTIR, FT–Raman and UV–Vis spectra of Temozolomide molecule. *J. Mol. Struct.* **1099**, 453–462 (2015).
84. Kumar Sahdev, A. et al. Chitosan-Folic Acid-Coated Quercetin-Loaded PLGA nanoparticles for hepatic carcinoma treatment. *Polym. (Basel).* **17**, 955 (2025).
85. Rahdari, T. et al. Advancing triple-negative breast cancer treatment through peptide decorated solid lipid nanoparticles for Paclitaxel delivery. *Sci. Rep.* **15**, 6043 (2025).
86. Zhu, Y. et al. Core–shell structural PLGA nanoparticle of Astaxanthin fabricated via micelle template for sustained release in vitro and long-term hepatoprotective effect in vivo. *J. Nanopart. Res.* **27**, 103 (2025).
87. Öztürk, A. A. & Arpagaus, C. Nano spray-dried drugs for oral administration: A review. *Assay. Drug Dev. Technol.* **19**, 412–441 (2021).
88. Dröge, W. Free radicals in the physiological control of cell function. *Physiol. Rev.* (2002).
89. Kim, S. J., Kim, H. S. & Seo, Y. R. Understanding of ROS-inducing strategy in anticancer therapy. *Oxid. Med. Cell. Longev* **2019**, (2019).
90. Kumar, M. et al. Formulation and evaluation of cetuximab functionalized phospholipid modified nanocrystals of Paclitaxel for non-small cell lung cancer therapy. *Sci. Rep.* **14**, 29114 (2024).
91. Kumar, M. et al. Fabrication of lipid-modified drug nanocrystals loaded injectable hydrogel for breast cancer therapy. *Discover Nano*. **20**, 30 (2025).


## Acknowledgements

This work has been supported by Anadolu University Scientific Research Projects Coordination under grant number TYL-2024-2735 (Project ID: 2735). The funders had no role in study design, data collection and analysis, decision to publish, or preparation of the manuscript. The authors would like to thank to Anadolu University, Faculty of Pharmacy, DOPNALAB for FT-IR analysis. The authors would also like to thank to corresponding authors' father A. Nurol Öztürk for providing DSC cells. We would also like to thank Deva Holding (Istanbul, Türkiye) for providing us with the Temozolomide. U-87 MG (HTB-14) and NIH/3T3 (CRL-1658) cell lines were purchased from the American Type Culture Collection (ATCC, Manassas, VA, USA). We confirm that all cell lines used in this study (U-87 MG human glioblastoma and NIH/3T3 mouse fibroblast) were commercially obtained from established and reputable sources. No human or animal tissue samples were collected directly from donors for this research. Therefore, the study did not involve any procedures requiring ethical approval from an institutional review board or animal ethics committee.

## Author contributions

The study's conceptualization and design were led by A.A.Ö. The pharmaceutical technology-related analyses, including data collection and evaluation, were conducted by Ş.Ş. and A.A.Ö. The biological activity studies were carried out by E.K.T. and M.B.; A.A.Ö. contributed to the discussion and interpretation of the results from both the pharmaceutical technology and biological activity studies. U-87 MG (HTB-14) and NIH/3T3 (CRL-1658) cell lines were purchased from the American Type Culture Collection (ATCC, Manassas, VA, USA). AAÖ wrote this manuscript with contributions of all co-authors. Author information: Şule Şahin (Ş.Ş.) Department of Pharmaceutical Technology, Faculty of Pharmacy, Anadolu University, Eskişehir, Türkiye. Elif Kaya-Tilki (E.K.T) Department of Pharmacology, Faculty of Pharmacy, Anadolu University, Eskişehir, Türkiye. Merve Baysal (M.B.) Department of Pharmaceutical Toxicology, Faculty of Pharmacy, Anadolu University, Eskişehir, Türkiye.A. Alper Öztürk (A.A.Ö)* Department of Pharmaceutical Technology, Faculty of Pharmacy, Anadolu University, Eskişehir, Türkiye. *Corresponding author. aaozturk@anadolu.edu.tr.

## Declarations

## Competing interests

The authors declare no competing interests.

## Additional information

**Supplementary Information** The online version contains supplementary material available at https://doi.org/10.1038/s41598-025-20012-x.

**Correspondence** and requests for materials should be addressed to A.A.Ö.

**Reprints and permissions information** is available at www.nature.com/reprints.

**Publisher's note** Springer Nature remains neutral with regard to jurisdictional claims in published maps and institutional affiliations.

**Open Access** This article is licensed under a Creative Commons Attribution-NonCommercial-NoDerivatives 4.0 International License, which permits any non-commercial use, sharing, distribution and reproduction in any medium or format, as long as you give appropriate credit to the original author(s) and the source, provide a link to the Creative Commons licence, and indicate if you modified the licensed material. You do not have permission under this licence to share adapted material derived from this article or parts of it. The images or other third party material in this article are included in the article's Creative Commons licence, unless indicated otherwise in a credit line to the material. If material is not included in the article's Creative Commons licence and your intended use is not permitted by statutory regulation or exceeds the permitted use, you will need to obtain permission directly from the copyright holder. To view a copy of this licence, visit http://creativecommons.org/licenses/by-nc-nd/4.0/.

© The Author(s) 2025

## Journal information

# SCIENTIFIC REPORTS

Publisher name: NATURE PORTFOLIO

### Journal Impact Factor ™

| 3.9 | 4.3 |
|---|---|
| 2024 | Five Year |

| JCR Category | Category Rank | Category Quartile |
|---|---|---|
| MULTIDISCIPLINARY SCIENCES *in SCIE edition* | 25/136 | Q1 |

**Source: Journal Citation Reports 2024.** Go to Journal Citation Reports

### Journal Citation Indicator ™

| 1.07 | 1.05 |
|---|---|
| 2024 | 2023 |

| JCI Category | Category Rank | Category Quartile |
|---|---|---|
| MULTIDISCIPLINARY SCIENCES *in SCIE edition* | 24/136 | Q1 |

Review Article 291

Open Access 261,490

Enriched Cited References 113,607

Clarivate Products

Journal Citation Reports™ Compare My favorites Sign In Register

Home > Journal profile

Favorite Export

JCR Year 2024

# Scientific Reports

Open Access since 2011

ISSN

2045-2322

EISSN

2045-2322

JCR ABBREVIATION

SCI REP-UK

ISO ABBREVIATION

Sci Rep

## Journal information

EDITION

Science Citation Index Expanded (SCIE)

CATEGORY

MULTIDISCIPLINARY SCIENCES

| LANGUAGES | REGION | 1ST ELECTRONIC JCR YEAR |
|---|---|---|
| English | ENGLAND | 2011 |

## Publisher information

| PUBLISHER | ADDRESS | PUBLICATION FREQUENCY |
|---|---|---|
| NATURE PORTFOLIO | HEIDELBERGER PLATZ 3, BERLIN 14197, GERMANY | 1 issue/year |

# Journal's performance

## Journal Impact Factor

The Journal Impact Factor (JIF) is a journal-level metric calculated from data indexed in the Web of Science Core Collection. It should be used with careful attention to the many factors that influence citation rates, such as the volume of publication and citations characteristics of the subject area and type of journal. The Journal Impact Factor can complement expert opinion and informed peer review. In the case of academic evaluation for tenure, it is inappropriate to use a journal-level metric as a proxy measure for individual researchers, institutions, or articles. Learn more